Low-Frequency, Motionally Induced Electromagnetic Fields in the Ocean
2. Electric Field and Eulerian Current Comparison

DOUGLAS S. LUTHER AND JEAN H. FILLOUX

Scripps Institution of Oceanography, La Jolla, California

ALAN D. CHAVE

AT&T Bell Laboratories, Murray Hill, New Jersey

The theoretical relationship between the motional horizontal electric field (HEF) and the seawater conductivity-weighted vertical average of horizontal water velocity is validated at subinertial frequencies with seafloor point measurements of HEF and moored measurements of horizontal water velocity collected in 1986–1987 in the central North Pacific during the Barotropic, Electromagnetic and Pressure Experiment (BEMPEX). The comparison is limited principally by inaccurate estimation of vertically averaged water velocity due to weak vertical coherences among the current meters and excessive rotor stalls at the deepest instruments. In the BEMPEX area, conductivity weighting results in only a trivial baroclinic contribution to HEF, so that HEF is an accurate measure of the vertically averaged water velocity (or, transport divided by depth) at periods greater than approximately 5 days. Furthermore, the actual transport divided by the depth is nearly identical to the barotropic (approximately depth-independent) component of motion. The magnetic field at the seafloor is found to have no detectable relationship to horizontal water currents at subinertial frequencies.

1. INTRODUCTION

The depth integral of horizontal water velocity (the transport) is one of the most fundamental characteristics of the general circulation of the oceans. Observation and theory now suggest that away from strong boundary currents (and even in some of these boundary regions) the transport can be dominated by the barotropic (nearly depth-independent) component of the flow. For example, in the recirculation region just south of the Gulf Stream, the mean currents have been found to be nearly depth-independent [*Schmitz*, 1980]. There are also many instances of fluctuating flows (for which depth-integrated currents and depth-independent barotropic currents are often equivalent) that have important if not dominant barotropic components. The nonlinear eddy field in the Gulf Stream recirculation region has only a weak depth dependence [*Schmitz*, 1978; *Hogg*, 1985], and the linear response of the mid-latitude oceans to direct atmospheric forcing at periods shorter than about 6 months is dominantly barotropic on the basis of both models [*Müller and Frankignoul*, 1981] and observations [*Niiler and Koblinsky*, 1985]. However, detailed information about the spatial distribution and variability of the barotropic velocity (and therefore the transport) is notably lacking by comparison with its baroclinic counterpart. This situation is predominantly the result of observational constraints; the baroclinic field has traditionally been determined by measurements of the density or temperature fields using hydrographic or bathythermographic surveys which are inherently insensitive to the barotropic component. Only two conventional tools to measure barotropic currents are available to the oceanographer. Long-duration observations of the barotropic velocity field can be achieved directly with strings of moored current meters, assuming that the barotropic field can be

discriminated from the often more energetic baroclinic components. This method is usually costly, especially if good resolution in the vertical (needed for separation of the barotropic and baroclinic components) and broad spatial coverage are desired. Barotropic fluctuations can also be inferred indirectly from the gradient of bottom pressure using geostrophy and assuming weak baroclinic pressure gradients at the bottom of the open ocean.

Unconventional technologies that measure the motional horizontal electric field (HEF) are also available for direct observation of the transport, but they remain underutilized. Such electric field measurements of transport are obtained from abandoned submarine communications cables [e.g., *Larsen and Sanford*, 1985; *Spain and Sanford*, 1987] or from self-contained bottom recorders. This paper presents observational justification for using the motional HEF to determine transport, with the emphasis on point measurements of HEF at the seafloor. Specifically, a detailed comparison is made between 10 month records of (1) HEF from the bottom of the North Pacific Ocean and (2) horizontal water velocity measured at six depths with mechanical current meters on a nearby subsurface mooring. This effort extends earlier work during the Mid-Ocean Dynamics Experiment (MODE) [*Cox et al.*, 1980] in which the total transport fluctuations obtained from 4 months of point HEF measurements were found to be similar to currents inferred from subsurface drifters. Thus the present intercomparison represents a more extensive test of the theoretical relationship between discrete stationary measurements of HEF and water currents in the open ocean than has been achieved previously.

The paper is organized as follows. The theoretical relationship between point measurements of the HEF and horizontal water velocity is briefly reviewed in section 2, which also contains definitions of the various integral measures of horizontal water velocity that will be discussed at various times in the text. The seafloor and mooring instruments and the HEF, water velocity, and hydrographic data employed in this study are described

in section 3. Potential flaws in the data sets are emphasized. Section 4 presents the comparison of fluctuations of the HEF with estimates from the mooring data of the fluctuations of the conductivity-weighted, vertical average (CWVA) of horizontal water velocity, to which the HEF is theoretically directly proportional. While the comparison is very good, there are disagreements due to a number of noise sources whose effects have been delineated with the help of ancillary data, such as acoustic tomography estimates of barotropic tidal currents. The comparison of the record means of HEF and CWVA water velocity and the comparison of the lowest frequency (1 cycle per year) variability that can be resolved are given special attention in section 5.

The lack of significant contributions to the HEF signals from depth-dependent currents is demonstrated in section 6, where it is also shown that barotropic motions, transport fluctuations, and CWVA water velocity variations are essentially identical in the BEMPEX area; hence HEF can be considered either a transport meter or barotropic current meter there. Section 7 summarizes the comparative results from this study with an emphasis on the disagreements and their demonstrated or probable causes. The fundamental conclusion from this study is that the HEF provides a more accurate measure of vertically integrated water velocity than can be obtained in the open ocean with a typical current meter mooring. This conclusion leads to high expectations for the oceanographic utility of HEF recorders, as is recounted in section 8.

2. MOTIONAL ELECTROMAGNETIC INDUCTION

The theory of motional electromagnetic induction in the ocean has been refined over the past few decades [e.g., *Sanford*, 1971; *Chave and Luther*, 1990]. Assuming distant continental boundaries and a flat seafloor with laterally homogeneous conductivity, then for the low frequency limit where the aspect ratio of ocean currents is small, where the effect of self-induction is weak, and where the vertical velocity can be neglected in comparison with the horizontal velocity, it can be shown [*Sanford*, 1971; *Chave and Luther*, 1990] that the point HEF is related to the horizontal velocity field by

$$\mathbf{E}_h = C \, F_z \, \hat{z} \times <\mathbf{v}_h>^* + \mathbf{N} \tag{1}$$

where C is a constant, F_z is the known local vertical component of the geomagnetic field (positive downward in the northern hemisphere), $\mathbf{N}$ is a vector noise term, and

$$<\mathbf{v}_h>^* \equiv \frac{\int_{-H}^{0} dz' \sigma(z') \mathbf{v}_h(z')}{\int_{-H}^{0} dz' \sigma(z')} \equiv <u>^* \hat{x} + <v>^* \hat{y} \tag{2}$$

is the vertically averaged, seawater conductivity-weighted horizontal water velocity, with $\mathbf{v}_h(z')$ as the depth-dependent horizontal water velocity. The asterisks in (2) denote conductivity weighting, and the angle brackets imply sea surface to seafloor integration and division by the water depth. Equation (2) reduces to the vertical average of horizontal water velocity (depth-normalized transport) when the seawater conductivity σ is depth-independent. Because of the cross-product relationship in (1) and the sign of F_z, the north electric field is proportional to the west component of $<\mathbf{v}_h>^*$, and the east electric field is

proportional to the north component of $<\mathbf{v}_h>^*$. To simplify subsequent discussion, the component of the HEF that is positive to the south (east) will be referred to as E^u_{-y} (E^v_x), so that from (1) and (2) E^u_{-y} (E^v_x) is proportional to $<u>^*$ ($<v>^*$), i.e., the subscript of the HEF component denotes the actual direction in which the component is positive and the superscript denotes the component of horizontal water velocity to which that electric field component is directly proportional.

Before proceeding, it is appropriate to reiterate some important terminology and relationships. The horizontal electric field (HEF or $\mathbf{E}_h$) vector is directly proportional to the quantity $<\mathbf{v}_h>^*$, specified by (2) as the CWVA of the horizontal water velocity vector. The simple vertical integral of horizontal water velocity is called the transport (or, more accurately, transport per unit width). For many oceanic regions, it can be expected that $<\mathbf{v}_h>^*$ is nearly equivalent to the vertically averaged horizontal water velocity $<\mathbf{v}_h>$, also called the depth-normalized transport, that is, the transport divided by the depth. The barotropic component of the flow, $\mathbf{v}_h^{bt}$, formally that component for which pressure and density surfaces coincide, is usually nearly depth-independent at subinertial frequencies, and is in many circumstances (such as in BEMPEX) nearly equivalent to both the depth-normalized transport $<\mathbf{v}_h>$ and the CWVA velocity $<\mathbf{v}_h>^*$. However, there are circumstances [e.g., *Fofonoff*, 1962] for which the barotropic velocity is only a component (in tandem with the baroclinic and nongeostrophic components) of the depth-normalized transport, and for which the depth-normalized transport differs from $<\mathbf{v}_h>^*$ owing to conductivity weighting of very strong near-surface currents. (Note that *Chave and Luther* [1990] used $\mathbf{v}_h^{bt}$ and $<\mathbf{v}_h>$ interchangeably for simplicity.) In subsequent discussion of the various water current functions, an estimate will be designated by a tilde, so that $\widetilde{<\mathbf{v}_h>}^*$ and $\widetilde{<\mathbf{v}_h>}$ are estimates of $<\mathbf{v}_h>^*$ and $<\mathbf{v}_h>$, respectively. Similarly, $\hat{\mathbf{E}}_h$ will denote observations of $\mathbf{E}_h$.

While (2) indicates that the HEF offers inherent vertical averaging of the horizontal water velocity, there is also lateral averaging that is not explicitly represented in (1) since it is unimportant under the assumption of small aspect ratio of the fluid motion. Formally, however, the multiplicative dependence of C and $<\mathbf{v}_h>^*$ in (1) must be replaced with a lateral convolution relation where C becomes an averaging kernel. A limiting form for this kernel is derived by *Chave and Luther* [1990], yielding a bound of a few times the water depth for the horizontal distance over which the water velocity is smoothed.

The oceanographic interpretation of (1) and (2) depends on the specific effects of the scale factor C, the seawater conductivity weighting in (2), and the noise term $\mathbf{N}$. The first of these is principally a function of the local seafloor electrical conductivity structure and is a measure of the extent to which electric currents induced in the ocean are shorted out by the underlying rock. C varies between 0 and 1 for the two limits of an infinitely conducting and a perfectly insulating seafloor, respectively. A detailed discussion of the electrical structure beneath the deep ocean floor is given by *Chave et al.* [1990a]. In summary, modern marine geophysical observations support a model of the seafloor conductivity consisting of a weakly conductive sediment and crustal layer of ~7 km thickness overlying a very resistive zone in the uppermost mantle. In this circumstance, the effect of electric current leakage into the seafloor is small, depending entirely on the integrated conductivity of the sediment and crustal region. Theoretical predictions suggest that C will lie between 0.9 and 1.0 for most of the deep ocean [*Chave and Luther*, 1990], and the limited available observations of both

HEF and concurrent horizontal velocity provide values of 0.91–0.94, assuming no baroclinic contribution to $<v_h>^*$, in the well-sedimented (and hence comparatively conductive) western North Atlantic [*Sanford et al.*, 1985; *Sanford*, 1986]. Most of the lateral variability in C will be due to changes in sediment thickness, and is unlikely to exceed 10%. A significantly larger range of C is expected near coastlines where a continental conductivity structure may predominate. For example, *Larsen and Sanford* [1985] and *Spain and Sanford* [1987] obtained values of C as low as 0.5, in comparing HEF with direct current measurements from the Florida Straits, due to the high conductivity of the ~4-km-thick sediments beneath the straits. While the lack of knowledge of C over the world oceans implies the need for collecting at least some direct current observations when HEF recorders are deployed (unless absolute current values are not required), the direct current observations can be widely spaced because C is unlikely to vary by more than 10% between geological extremes along the ocean floor, but most importantly, once C is established at a location it is known forever.

The seawater conductivity weighting in (2) acts like a low-pass filter applied to the vertical structure of the horizontal water velocity. The strength of the filtering can be examined by expanding the conductivity and velocity in terms of orthogonal vertical structure functions, making the integral in the numerator of (2) a trivial summation of products of amplitude coefficients. For example, using the dynamical vertical structure functions appropriate for horizontal currents at low frequencies [e.g., *LeBlond and Mysak*, 1978, section 15], Table 1 gives the first four amplitude coefficients (barotropic plus first three baroclinic modes) in the structure function expansions of four conductivity profiles computed from zonally averaged temperature and salinity profiles [*Levitus*, 1982]. The buoyancy frequency data needed to numerically compute the structure functions was also taken from *Levitus* [1982] for the appropriate latitude bands. If the amplitude coefficients of a similar expansion of horizontal water velocity were all identical, then the coefficients in Table 1 would indicate the relative contributions of the various horizontal current modes to $<v_h>^*$. In general, the barotropic mode is more exactly preserved and the baroclinic components are increasingly downweighted as the latitude increases, a consequence of the interplay between the poleward decrease in surface heat content and the dominance of conductivity by temperature (Figure 1). Even in the worst case, the seawater conductivity filter strongly emphasizes the barotropic mode; for instance, for the tropical and sub-tropical cases of the first two columns of Table 1, the first baroclinic mode would have to have approximately 10 times the amplitude of the barotropic mode in order to produce an electric field equivalent to that produced by the barotropic mode. Further discussion and quantification using actual current observations are given by *Chave and Luther* [1990]. The HEF should serve as an effective
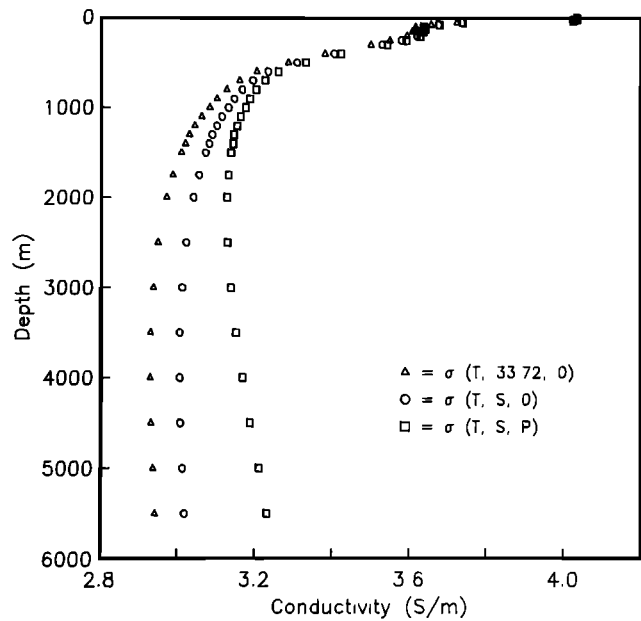

Fig. 1. Conductivity profiles demonstrating the dependence of conductivity on, in order of importance, temperature, pressure, and salinity. The basic data are averages of temperatures and salinities from two CTD profiles taken near the BEMPEX mooring on September 2, 1986, and May 16, 1987. Conductivity was calculated using the empirical formulas provided by *Fofonoff and Millard* [1983]. The left profile results from assuming constant salinity (set at 33.72‰) and constant pressure (0 dbar). The middle profile results from assuming only constant pressure (0 dbar). The right profile incorporates all the data at their proper pressures.

barotropic current meter in most of the world oceans because of the inherent vertical averaging in (2) and the physical behavior of seawater conductivity with depth and because the barotropic and baroclinic components of motion are generally of comparable magnitude.

The noise term in (1) contains components due to nonlocal motional electric fields, external (ionospheric and magnetospheric) electromagnetic sources, and random effects. The first part is discussed extensively by *Sanford* [1971]. Its most important component in the open ocean is due to large-scale horizontal divergence of $<v_h>^*$. *Chave and Luther* [1990] argue that this divergence component is very small owing to the structure of the lateral averaging kernel. Contributions from local topography and oceanic boundaries deserve greater theoretical attention, although at least in some practical instances they do not appear to pose a serious problem; for example, *Larsen and Sanford* [1985] and *Spain and Sanford* [1987] have successfully applied (1) and (2) in the Florida Straits. Externally generated electric field noise is empirically well understood to have a limited effect at a period of a day and a negligible effect at periods longer than 5 days. This is demonstrated [*Chave et al.*, 1989] by examining the spatial variability of the coherence structure of the seafloor electric and magnetic fields (see also section 4 below). The externally induced part of the HEF is removable using frequency domain correlation or time domain adaptive cancellation techniques, with the magnetic field (which contains no detectable motional component; see section 4) as a measure of the noise.

3. INSTRUMENTS AND DATA

The HEF data discussed in this paper were collected during the Barotropic, Electromagnetic and Pressure Experiment (BEM-

TABLE 1. Vertical Mode Amplitude Coefficients From Conductivity Profile Expansions

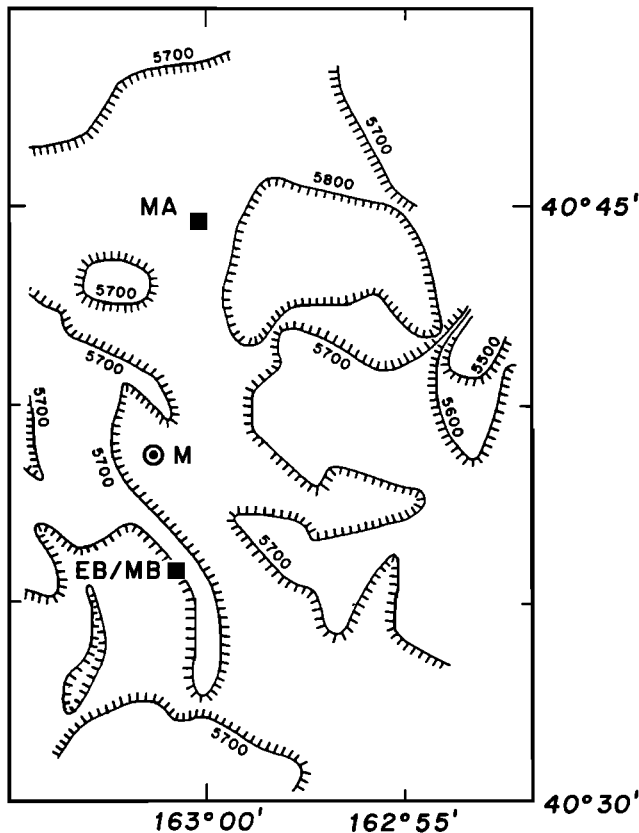| Mode	12.5°N Pacific	32.5°N Atlantic	42.5°N Pacific	57.5°S Atlantic
1	3.302	3.522	3.181	3.036
2	–0.334	0.419	0.053	–0.012
3	0.116	–0.051	0.067	–0.029
4	0.002	–0.043	–0.007	–0.013

Values are in Siemens per meter.

Fig. 2. Instrument locations superimposed on the bathymetry (in uncorrected meters). The locations of the mooring (designated "M"), electric field recorder EB and magnetometers MA and MB are shown. The bathymetry was mapped during deployment of the seafloor instruments using the R/V *New Horizon's* echo sounder with intermittent satellite navigation. Therefore the bathymetry should be interpreted not as literally correct, but only as indicative of the environment.

PEX) in the central North Pacific during 1986–1987. BEMPEX utilized an approximately 1000 km by 1000 km array of seafloor electromagnetic and pressure instrumentation to study a variety of oceanic and geophysical phenomena. The motivation for and scientific goals of BEMPEX were discussed in the prerecovery overview by *Luther et al.* [1987]. A preliminary comparison of the HEF and mooring data was presented by *Chave et al.* [1990*b*], and initial analyses showing high coherence between low frequency barotropic motions (as represented by the seafloor electric field and pressure observations) and surface atmospheric air pressure and wind stress curl are given by *Luther et al.* [1990].

BEMPEX included a single, taut-wire, subsurface mooring, carrying six mechanical current meters, that was deployed at 40.647°N, 163.025°W, in 5751 m of water in early September 1986 and recovered in September 1987. A seafloor HEF recorder was placed (Figure 2) approximately 6 km south of the mooring at 40.597°N, 163.013°W in 5730 m of water in August 1986 and recovered in June 1987. The electric field recorder and current meter mooring were sufficiently proximate to ensure that the mooring was within the horizontal averaging domain of the electric field recorder. Two seafloor three-component magnetometers were also located nearby (Figure 2). The magnetometers are used for studying crustal conductivity and delineating the frequency domain where externally generated fields dominate the HEF observations. The observed magnetic fields

are not expected to have any significant oceanically generated signals, and this is confirmed below. The topography of the immediate area around the mooring consists of low (≈100 m) abyssal hills and valleys with minimal sediment drape; the nearest larger scale feature is the Surveyor Fracture Zone, with 500 m maximum relief occurring about 60 km to the northeast.

The self-contained, seafloor-based horizontal electrometers and magnetometers are proven designs developed by one of us [*Filloux*, 1987] that have been used successfully at sea numerous times over the past decade, primarily for geophysical studies based on the theory of downward diffusion through the solid Earth of high frequency (0.01 to 10 cph) electromagnetic fields generated in the ionosphere and magnetosphere. The instruments operate in a free-fall mode and are self-buoyant, returning to the surface upon timed release of an anchor tripod. The horizontal electrometer records the electric potential across two orthogonal 6-m-span salt bridges at a selectable sampling rate (16 samples per hour in the present case) and utilizes an electromechanically activated electrode reversing ("chopping") technique to cancel an otherwise hopelessly large and time-variable electrode bias. The chopping technique simultaneously corrects for electronic and power supply drifts as well. This means that the HEF is referred to a true zero datum. Calibration of the electrometers before and after deployment involves verifying the voltage-to-frequency conversion factor (to date these electronic components have been trouble-free) and verifying that the chopper's open state switch resistance is large (> 500 KΩ) with respect to the overall salt bridge resistance of ~5 KΩ [*Filloux*, 1987].

The magnetometers simultaneously sense all three magnetic field components by means of magnets suspended on torsion fibers in feedback coils. Optical sensors detect the positions of the magnets, and the currents in the feedback coils are adjusted to produce the torque necessary to null the deflections caused by the ambient magnetic variations. The measured coil current is linearly proportional to the magnetic variations.

The orientations of the seafloor instruments with respect to magnetic north, as well as the instrument tilt, are internally recorded. After recovery, the recorded horizontal electric fields and three-component magnetic fields are rotated to local geographic reference frames using the magnetic declination appropriate for each site. The declinations were obtained from the IGRF85 map of Earth's permanent magnetic field at the sea surface, updated for secular variations to January 1, 1987. The accuracy of the final orientations is ±1°.

The subsurface mooring was assembled by the Instrument Development Group (IDG) at Scripps Institution of Oceanography (SIO). The mooring was supported by a single 41-inch hollow steel sphere at 64 m depth and thirty-four 17-inch glass spheres distributed along its length. The top 1950 m of the mooring was 1/4-inch wire rope with 1/4-inch Kevlar rope used below about 2000 m depth. IDG's vector measuring current meters (VMCMs) were located at depths of approximately 73, 173, 943, 2498, 5650, and 5722 m; these depths were chosen for redundancy near the surface and seafloor and for uniform spacing in buoyancy frequency scaled (stretched) coordinates in the interior. C. S. Draper Laboratory temperature and pressure (T/P) recorders [*Wunsch and Dahlen*, 1974] were placed at depths of 70 m and 293 m to monitor mooring motion and accurately specify depths of the upper ocean instruments. Mooring motion was comparatively small, with vertical excursions exceeding 10 m only occasionally during the passage of inertial-internal waves. The maximum vertical excursion of the

top of the mooring was 28 m, and the standard deviation of the vertical motion was 2.7 m for the entire year-long deployment. The majority of this variability was due to inertial oscillations and a low-frequency drift in the pressure records. Excluding the low-frequency drift, subinertial vertical deflections of the top of the mooring rarely approached 3 m. Since the vertical shear of the horizontal currents was always weak, the relatively minor mooring motion observed did not warrant any attempt at correcting measured currents for the vertical deflections.

The VMCM was designed for accurate near-surface measurement of low-frequency ocean currents in the presence of high-frequency surface wave and mooring motions [Weller and Davis, 1980]. Each instrument has two orthogonal propeller-type paired rotors each with a rated stall speed of 1 cm s^{-1} or more, depending on bearing loads induced by motions orthogonal to the rotor axis. In the deep North Pacific, total current speeds including inertial oscillations were frequently less than 2 cm s^{-1}, resulting in substantial rotor stalling for the three deepest instruments on the BEMPEX mooring. For example, a month of raw current data is presented in Figure 3 that shows increasingly more frequent occurrences of zero speeds as depth increases.

Near the surface, typically only 20% of the observations (for each horizontal current component) that had speeds less than .5 cm s^{-1} were zero, yielding a total of less than 1% of all observations that were zero; whereas, near the bottom, 60% to 70% of the current observations that had speeds less than 0.5 cm s^{-1} were zero, yielding a total of 25% to 35% of all observations that were zero.

Furthermore, the VMCMs used in BEMPEX internally recorded only the averaged magnetic east and north components of current every half hour, so that the occurrence of a single rotor stall (as opposed to both rotors stalling) is undetectable after the fact. As will be shown, barotropic currents estimated from the BEMPEX mooring are weaker than those derived from the HEF, a result which is not due to HEF measurement error (as shown below) but is attributed to rotor stalling and other weak-current biases [Weller and Davis, 1980] in the deepest VMCMs. Vertical coherence among the VMCM currents may also be degraded by the rotor stalling, introducing noise into vertical mode decompositions, since the independent rotors can each stall at different times during an averaging interval. Despite the large numbers of rotor stalls at the deepest instru-
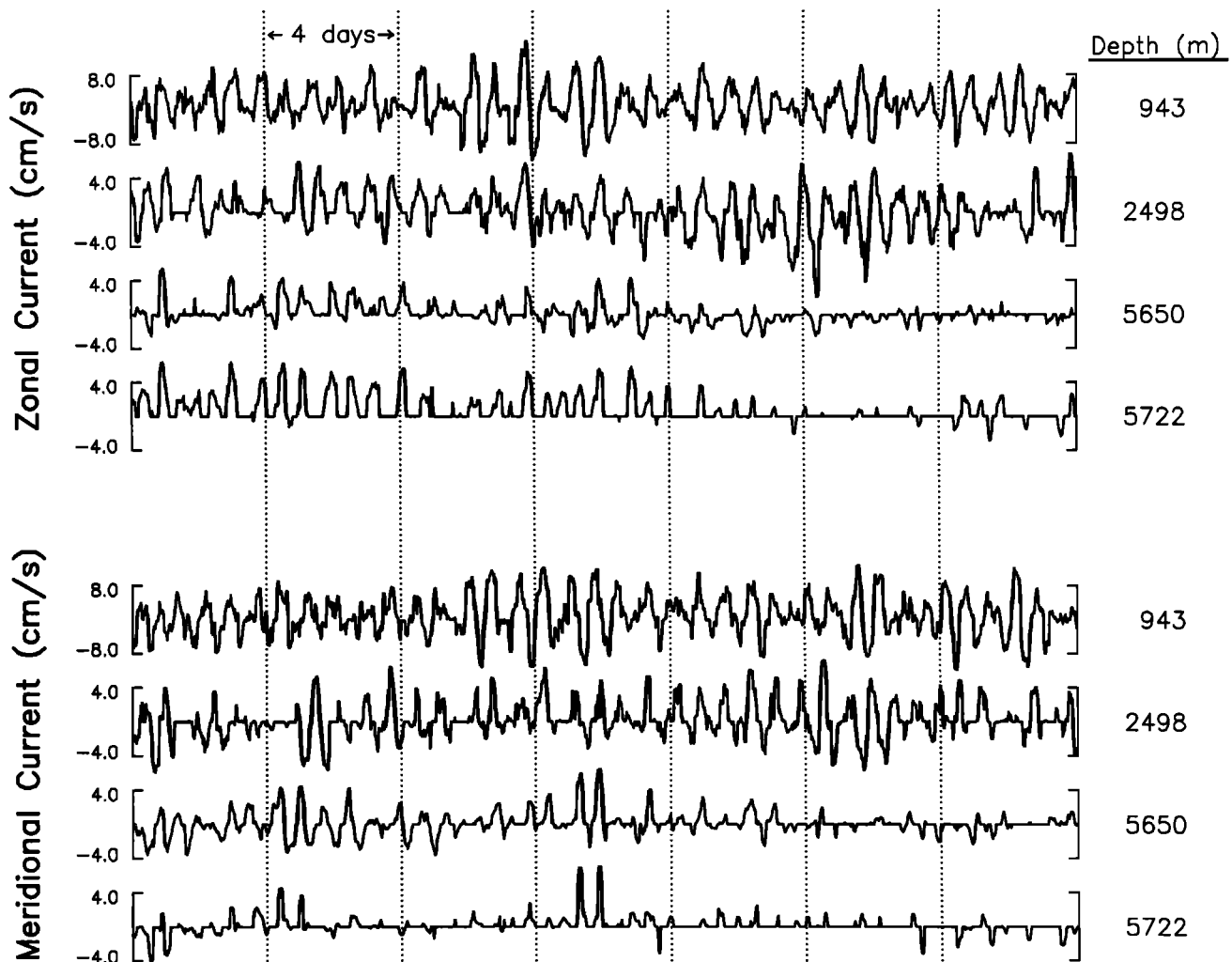

Fig. 3. Zonal and meridional currents observed from the four deepest VMCMs on the BEMPEX mooring during the month of May 1987. Vector averages were stored every half hour. All the stored values have been plotted. Vertical dotted lines have been plotted every 4 days. Note the large numbers of zero values as depth increases. The apparent tendency toward nonnegative values at the deepest instruments (especially for the zonal component) is not construed as an instrumental bias but rather is the result of superimposing inertial oscillations on a low-frequency current that is positive during the month of May (see Figure 4a).

ments, no other current meter technology is obviously superior for measuring deep ocean currents (e.g., see the intercomparison by *Weller and Davis* [1980]).

Figure 4 displays low-pass-filtered currents from the BEMPEX mooring and low-pass filtered electric fields from the nearby HEF instrument, EB (Figure 2). The currents clearly show a strong inclination toward barotropic motions which are visually correlated with the electric field records. Note that the currents from 5650 m are decidedly less energetic (more so in the zonal component) than the currents from the nearby instrument at 5722 m or the more distant instrument at 2498 m. The reduction in variance occurs at all frequencies from the lowest resolvable one up to the Nyquist (e.g., Figure 5) and cannot be explained by boundary layer, boundary reflection, or bottom trapping theories which predict enhancement of fluctuation amplitudes near the boundary in only specific narrow frequency bands associated with their differing physical processes. In any case, the deepest instrument was located approximately 29 m off the bottom and therefore was probably not often in the frictional boundary layer, whose thickness was found to be less than 35 m in the more energetic western North Atlantic [*Armi and D'Asaro*, 1980]. No significant difference between either velo-

city ellipse orientation or coherence phase lag between the two deepest instruments is observed at long periods (>1 day), further suggesting that boundary layer effects are absent. The most plausible explanation for the reduced variance at 5650 m is higher than normal rotor bearing friction (L. Regier, private communication, 1989).

The remainder of this paper will focus on the time period of overlap of the HEF data from instrument EB and the current meter data from the BEMPEX mooring, i.e., September 2, 1986, 1920 UT to June 19, 1987, 1920 UT.

The seawater conductivity profile required to calculate the conductivity-weighted, vertically averaged water velocity in (2) was obtained using a variety of information. Three nearly full-depth conductivity-temperature-depth (CTD) profiles were collected near the BEMPEX mooring on cruises in September 1986 and May and September 1987, and examined for consistency by comparison with historical means taken from *Levitus* [1982]. The *Levitus* [1982] temperatures and salinities were converted to conductivities using the empirical relations provided by *Fofonoff and Millard* [1983], and assuming that the reference conductivity $\sigma(35\%_0, 15^0C, 0$ dbar$) = 4.2896$ S m^{-1} [*Horne*, 1969]. In typical oceanographic settings, conductivity is most dependent
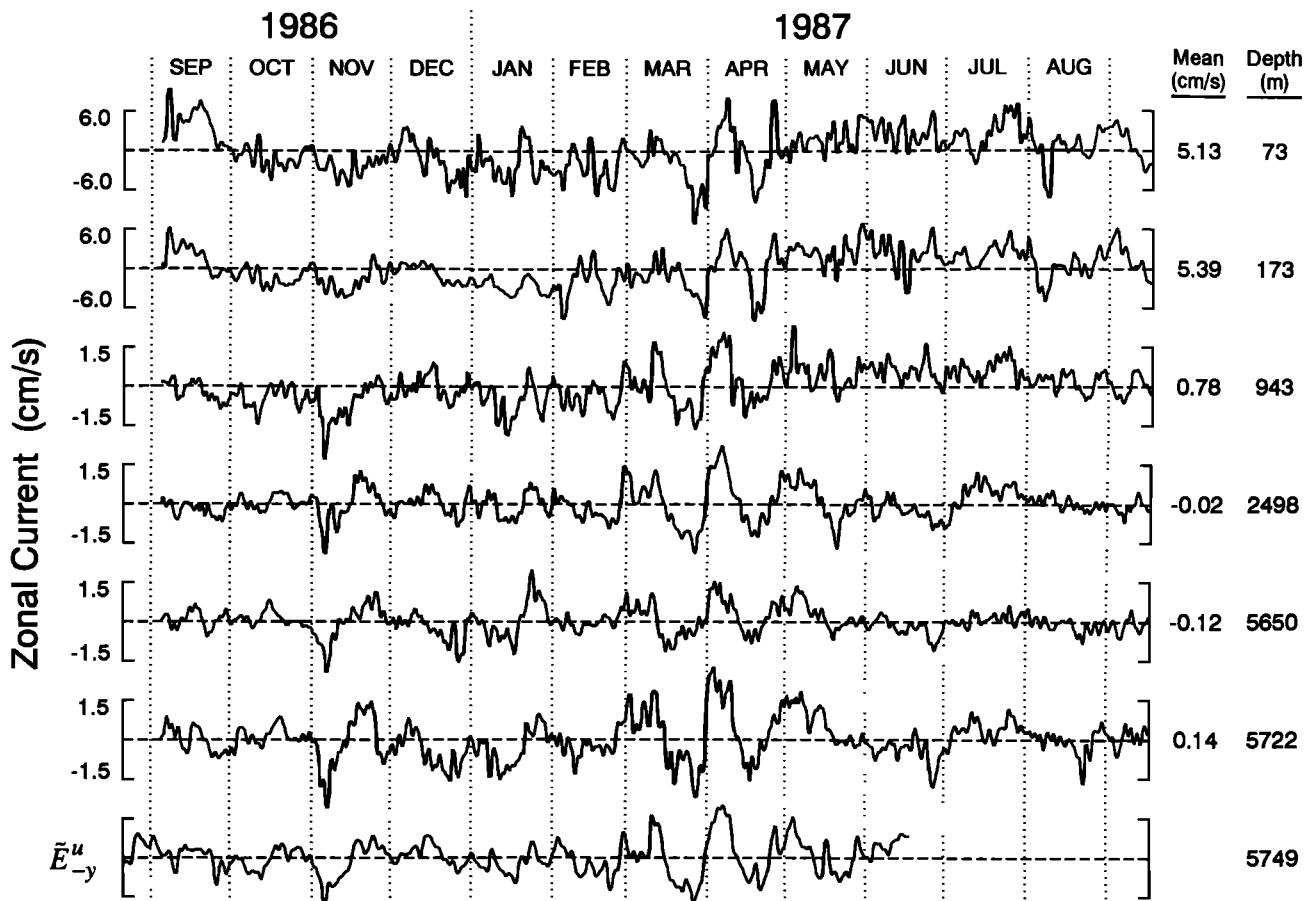

Fig. 4a

Fig. 4. (a) The top six frames show low-pass-filtered (3 dB point at 2.7 days, 20 dB point at 1.6 days) zonal currents from the BEMPEX mooring with means subtracted. The mean and depth for each record are indicated to the right of each frame. The ordinate range for the top two frames is larger than the range for the next four. The bottom frame shows the low-pass-filtered south component (called $\tilde{E}^u_{-y}$) of the horizontal electric field (in arbitrary units and with the mean subtracted) measured approximately 6 km south of the mooring. (b) As in Figure 4a, except for the meridional component of water velocity and the east component (called $\tilde{E}^v_x$) of the horizontal electric field. Notice that much of the variability in the currents is visually correlated and in phase across thousands of meters of depth, implying the existence of appreciable barotropic signals. These vertically coherent signals are replicated to a high degree in the electric field data.
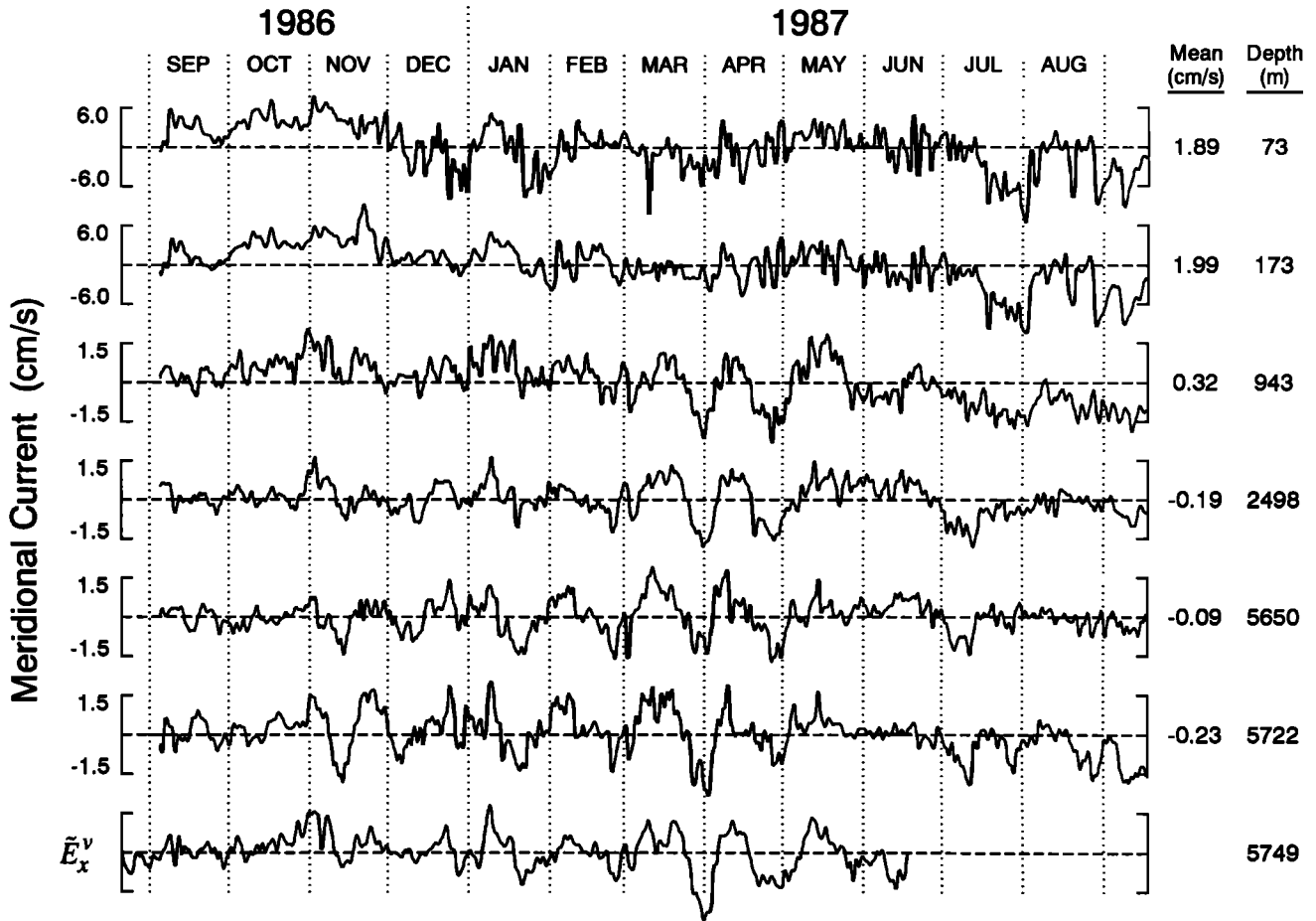
Fig. 4b

upon temperature, followed by pressure and then salinity (Figure 1). Figure 6 compares the conductivity profiles from the three CTDs taken near the BEMPEX mooring with the calculated conductivity profiles for the mean Levitus [1982] data from the

Frequency (cph)

two 5° squares that encompass most of the BEMPEX area. The CTD data is most consistent with the 5° square that encircles the CTD locations. All the conductivity profiles are essentially identical below 1500 m. Figure 1 displays a top to bottom profile; note that the range of conductivity from top to bottom is only about 25% of the overall mean.

Temperature time series from the moored VMCMs and T/P gauges were combined with average salinities from the September 2, 1986, and May 16, 1987, CTDs to yield time series of conductivity. These conductivities varied significantly during the experiment only above 200m. Even in this depth range, the maximum temporal fluctuation of conductivity about the mean was only 20% of the mean. The conductivity profiles from the September 2, 1986, and May 16, 1987, CTDs (Figure 6) closely coincide, at each VMCM and T/P depth, with the 1-standard-deviation limits of the conductivity time series.
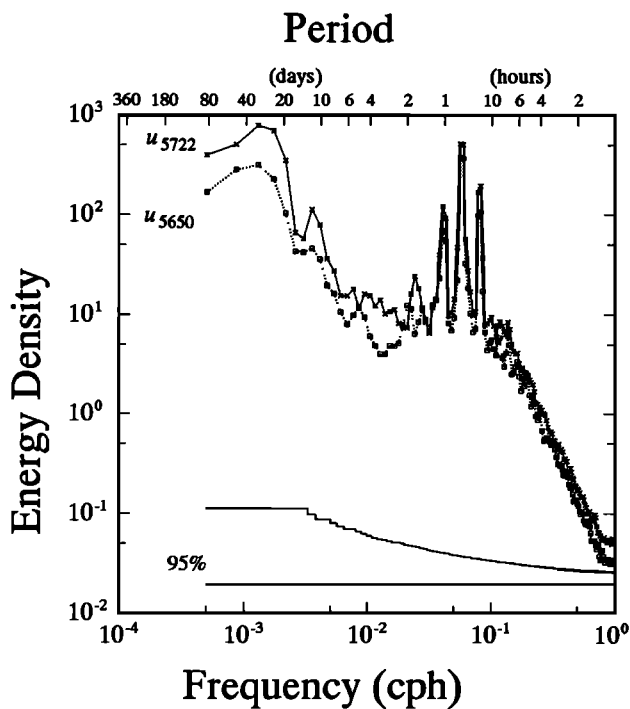
Fig. 5. Power spectra of zonal currents at 5650 m (lower, dotted line with squares) and 5722 m (upper, solid line with crosses) from the BEMPEX mooring. The weaker current at all frequencies at the slightly shallower instrument is probably due to excessive rotor bearing friction. The lengths of the records used for these spectra are each 6960 hours. Every other plotted point is independent (i.e., 50% overlap of frequency band averaging of FFT-derived periodogram). The 95% confidence intervals for each independent point are given at the bottom. The intervals decrease with increasing frequency due to increasing band averaging. The spectrum has units of (cm/s)^2/cph and is normalized so that the power of a unit amplitude sine wave is 1.
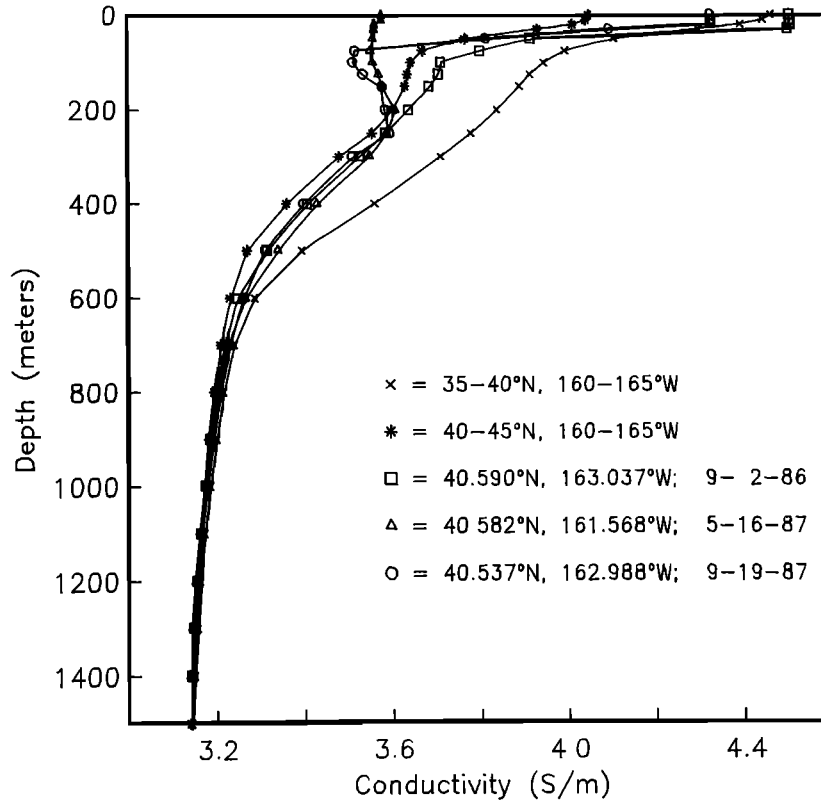
Fig. 6. Upper ocean conductivity profiles from CTD data taken near the BEMPEX mooring on the dates indicated, and from climatological mean temperatures and salinities [*Levitus*, 1982] for 5° squares encompassing the BEMPEX area. Note that the CTD data are most consistent with the 5° square that encircles the CTD locations.

4. COMPARISON OF $<\widetilde{v_h}>^*$ WITH $\tilde{E}_h$

The continuous vertical integrals in (2) were first approximated by application of the trapezoidal rule to each pair of VMCM velocity and associated conductivity time series, where it was also assumed that there was no velocity shear or conductivity gradient above 73 m or below 5722 m. While the temporal and vertical variation of the conductivity enters explicitly into (2), $<\widetilde{v_h}>^*$ was found to be very insensitive to the weak temporal variability of the conductivity described above and only slightly sensitive to the vertical gradient of conductivity. It will be shown later that this insensitivity to the conductivity profile is the result of relatively strong depth-independent (barotropic) currents combined with the relatively small variation of conductivity with depth. Consequently, for the remainder of this paper the mean conductivity profile, determined from the time mean of the conductivity time series at each current meter, will be used in estimates of the terms in (2).

A number of alternative discrete approximations to the integrals in (2) were tested in an attempt to maximize the coherence between $\tilde{E}_h$ and $<\widetilde{v_h}>^*$ and thereby arrive at a "best" estimate of $<v_h>^*$ from the current meter data. While the changes in the coherence functions were always slight, and certainly not significant at the 95% confidence level, they were consistent across the low-frequency band. For instance, deleting the 5650-m instrument, which had much reduced variance relative to the 5722-m instrument as discussed above, improved the coherence but not as much as was obtained by employing point-by-point averaged series of the two near-bottom records. This combination appears to have mitigated some of the effects

of the rotor stalling. Deleting the 73-m instrument degraded the coherence, but restricting the depth of influence of the 173-m instrument to only 250 m improved the coherence; in essence, the trapezoidal rule was altered in the 173-m to 943-m depth interval where the near-surface currents appear not to be representative of in situ currents to as great a depth as the ordinary trapezoidal rule allows.

In summary, a discrete approximation to (2) at each point in time, namely,

$$<\widetilde{v_h}>^* \equiv \frac{\sum_{n=1}^{5} v_{h,n} \, \bar{\sigma}_n \Delta z_n}{\sum_{n=1}^{5} \bar{\sigma}_n \Delta z_n} \equiv <\widetilde{u}>^* \hat{x} + <\widetilde{v}>^* \hat{y} \qquad (3)$$

was chosen that employs distinct but time-invariant values for the conductivity at each current element (Table 2), an averaged time series from the two near-bottom current meters, and that

TABLE 2. Elements for Equation (3), the Discrete Approximation to $<v_h>^*$

n	Instrument Depth, m	$\bar{\sigma}_n$, S m^{-1}	Δz_n, m
1	73	3.654	123
2	173	3.624	127
3	943	3.180	1470
4	2498	3.128	2372
5	5686[a]	3.241	1659

[a]Average depth of the two near-bottom current meters.

a

Period

b

Period

restricts the surface currents, as measured by the two shallowest current meters, to the top 250 m. No claim is being made that this is the "optimum" approximation to (2) given the vertically discrete observations, but it is simple and has yielded good results. It should be emphasized again that other integration schemes yield comparable results, and the present conclusions do not depend on the manner in which (2) is estimated, as will become clear later.

Figure 7 presents the coherence functions between the Cartesian components of $<\tilde{v}_h>^*$ and the corresponding components of $\tilde{E}_h$. The coherence amplitude is above the 95% level of zero significance at periods greater than 5 days except in a few relatively narrow frequency bands, while the coherence phase is not significantly different from zero, except at 6 days for the zonal component (Figure 7a) where the phase just barely differs from zero with 95% confidence. The coherence amplitudes in Figure 7 are greater than the coherence amplitudes between $\tilde{E}_h$ and the individual current meter records, with only a single (hence, statistically trivial) exception at 5 days in the coherence between meridonal velocity at 943 m and $\tilde{E}_x^v$.

The lack of coherence in Figure 7 at periods shorter than 5 days could be due to external geomagnetic noise, since electromagnetic fields generated in the ionosphere and magnetosphere are known to have significant amplitudes at the seafloor at periods under a few days. Magnetotelluric theory predicts that orthogonal electric and magnetic field components will be highly coherent when externally induced fields are large. Figure 8a shows an example of the coherence between orthogonal electric and magnetic fields near the BEMPEX mooring (from
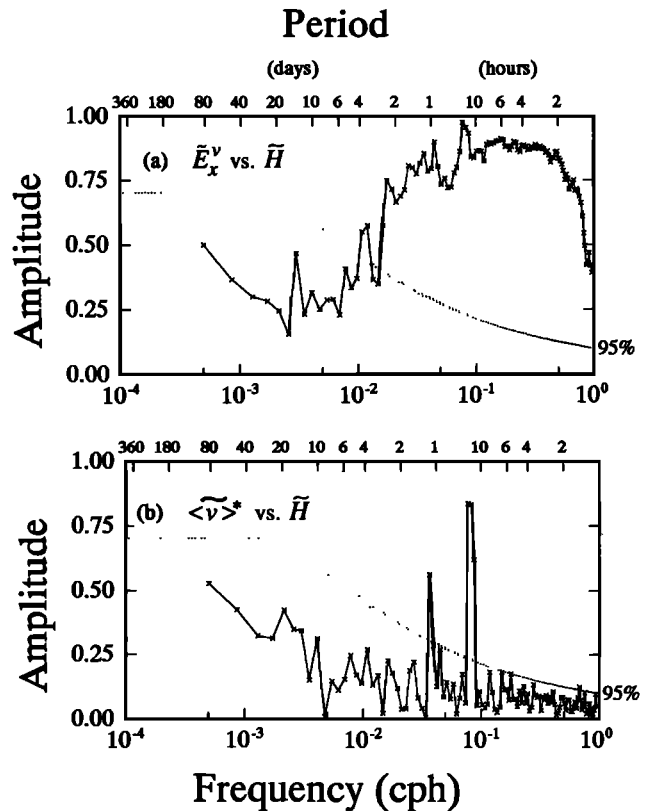
Period

Fig. 7. (a) Coherence amplitude and phase between $<\tilde{u}>^*$ and $\tilde{E}_{-y}^u$. Every other plotted point is independent and a positive phase indicates that $<\tilde{u}>^*$ leads $\tilde{E}_{-y}^u$. The lengths of the records used for this coherence are each 6960 hours. The dashed line in the amplitude plot is the level of no significance at 95% confidence. (For the definition of $<\tilde{u}>^*$, see equation (2).) (b) As in Figure 7a, except for $<\tilde{v}>^*$ and $\tilde{E}_x^v$. (For the definition of $<\tilde{v}>^*$, see equation (2).)

Fig. 8. (a) Coherence amplitude between the east component of the horizontal electric field ($\tilde{E}_x^v$) measured by EB and the north component, $\tilde{H}$, of the magnetic field measured by MB (Figure 2). Plotted as in Figure 7. (b) Coherence amplitude between $<\tilde{v}>^*$ and the north component of the magnetic field measured by MB. Plotted as in Figure 7.
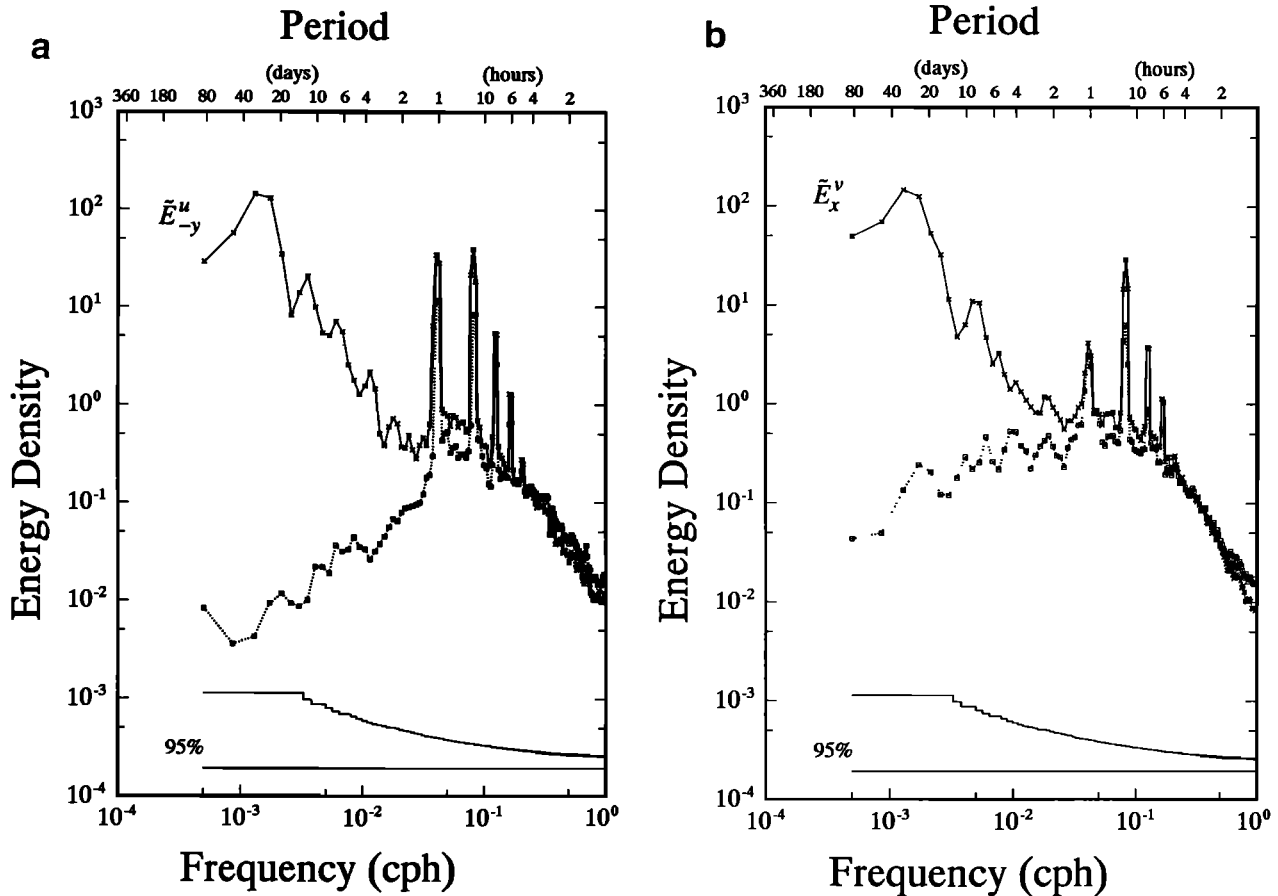
Fig. 9. (a) Power spectra of the south component ($\tilde{E}^u_{-y}$) of the horizontal electric field measured by EB (solid line with crosses) and the calculated south electric field due to external sources (dotted line with squares). Units are $(\mu V/m)^2/cph$. Otherwise, plotted as in Figure 5. (b) Power spectra of the east component ($\tilde{E}^v_x$) of the horizontal electric field measured by EB (solid line with crosses) and the calculated east electric field due to external sources (dotted line with squares). Plotted as in Figure 9a.

instruments EB and MB in Figure 2). The strong correlation between the electric and magnetic fields is clear evidence of a nonoceanic origin of the electric field signals at periods less than a few days, because the seafloor magnetic field does not contain a significant oceanic component, as expected from theory [*Chave and Luther*, 1990] and prior observations [e.g., *Chave et al.*, 1989], and as demonstrated by the lack of coherence between the magnetic field and $<\widetilde{v_h}>^2$ (e.g., Figure 8b) or between the magnetic field and any of the individual current measurements (not shown). An exception to this statement must be made for the tides, however, since as deterministic signals extant in ocean currents and electromagnetic fields from a variety of sources, the tides can produce high coherence among the variables (e.g., the diurnal and semidiurnal peaks in Figure 8b) irrespective of whether direct physical relationships exist. Actually, non-cross-spectral evidence exists that shows that the nonsolar tidal constituents in electric and magnetic field data collected in and near the oceans are induced by oceanic tides [e.g., *Larsen*, 1968].

Since the magnetic field serves as a proxy for the geomagnetic noise, an adaptive correlation canceler [*Widrow et al.*, 1975] was devised to remove that part of the HEF time series that is correlated with the vector magnetic field, after filtering the data through a low-pass filter with a sharp cutoff at 1.5 days to remove tidal and solar daily variations. This reduced the

coherence between $\tilde{E}_h$ and the magnetic field to below the zero significance level at periods longer than 2 days, but had little effect on $\tilde{E}_h$ versus $<\widetilde{v_h}>^2$ coherence at periods of 2 to 5 days, suggesting that other processes are producing the vanishing coherence at 2–5 days seen in Figure 7.

To graphically illustrate the small probable contribution of geomagnetic noise to the variability of $\tilde{E}_h$ at periods greater than 2 days, magnetotelluric transfer functions between $\tilde{E}_h$ and the observed magnetic field from instrument MB in Figure 2 have been calculated from an assumed Earth conductivity structure based on a number of geophysical studies. The result is the estimate of the externally produced electric fields shown in Figure 9. The method of calculation of the transfer functions is described in the appendix and is dependent upon a conservative model for the conductivity structure of the Earth. If larger conductivities in the lower mantle are assumed, for which there is increasing evidence, the externally generated electric fields at periods greater than 2 days will be weaker than those shown in Figure 9. Assuming smaller conductivities in the lower mantle and below does not result in electric fields comparable to the observations at periods greater than 2 days. Even assuming the deep interior of the Earth is an insulator, in contradiction to geophysical observations, results in only "white" spectral levels for the predicted electric fields at periods greater than 2 days, still well below the observed "red" electric fields. Note the

good agreement in Figure 9 between the observed and predicted electric fields at nontidal periods shorter than 12 hours, indicating a reasonable accuracy for the conductivity model in the upper mantle and crust. At periods greater than 2 days, the largest contribution to the observed electric fields from the externally produced fields is, from Figure 9, expected to be no more than 40% of the energy in the east ($\tilde{E}_x^v$) electric field component in the 2- to 5-day band (Figure 9b), and is generally much less than 10% both for $\tilde{E}_x^v$ at longer periods and for $\tilde{E}_{-y}^u$ at all periods greater than 3 days.

While the coherence between $\tilde{E}_h$ and $\langle\widetilde{v_h}\rangle^*$ at periods greater than 5 days is high (Figure 7), the coherence amplitude is not unity and occasionally slips below the 95% level of no significance. It is reasonable to wonder whether these features represent inherent inaccuracies in either equation (1) or in the measurement of E_h, or whether they are due to inaccuracies in estimating $\langle v_h\rangle^*$ from a discrete approximation like (3) with noisy current meter data. The latter appears to be the case. The coherence between neighboring pairs of current meters is often below the 95% level of no significance at periods greater than 1 day. At worst there is no significant vertical coherence at all, as for instance between the meridional velocity measured at 173 m and 943 m (Figure 10). The coherences between currents measured at 2498 m and near the bottom are especially revealing (Figure 11). The zonal current coherence is weakest at 80, 15, and 8 days, exactly where the coherence between $\tilde{E}_{-y}^u$ and $\langle\widetilde{u}\rangle^*$ is small (see Figure 11a). Similarly, the meridional current coherence (Figure 11b) is weakest over 50–80 days and at 12 days, exactly where the coherence between $\tilde{E}_x^v$ and $\langle\widetilde{v}\rangle^*$ is small. Note also that the inter-element coherences in Figure 11 are insignificant at periods of 2–5 days, commensurate with the lack of coherence between $\tilde{E}_h$ and $\langle\widetilde{v_h}\rangle^*$ in that band. The coherence between $\tilde{E}_h$ and $\langle\widetilde{v_h}\rangle^*$ has greater amplitude at periods greater than 5 days than any of the interelement moored current coherences, including the near-surface and near-bottom pairs, with only occasional exceptions at isolated periods.

The low vertical coherence between the moored current meters is the principal evidence for the assertion that the limiting factor in the comparison of $\tilde{E}_h$ and $\langle\widetilde{v_h}\rangle^*$ is the inaccuracy in (3) of estimating $\langle\widetilde{v_h}\rangle^*$ from a few discrete measurements of the velocity field. The lack of vertical coherence between current meters cannot be ascribed solely to rotor stal-
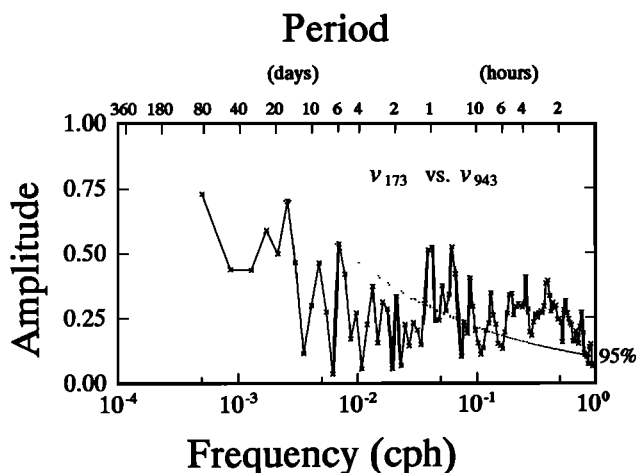

Fig. 10. Coherence amplitude between meridional currents measured at 173 m and 943 m on the BEMPEX mooring. Plotted as in Figure 7.
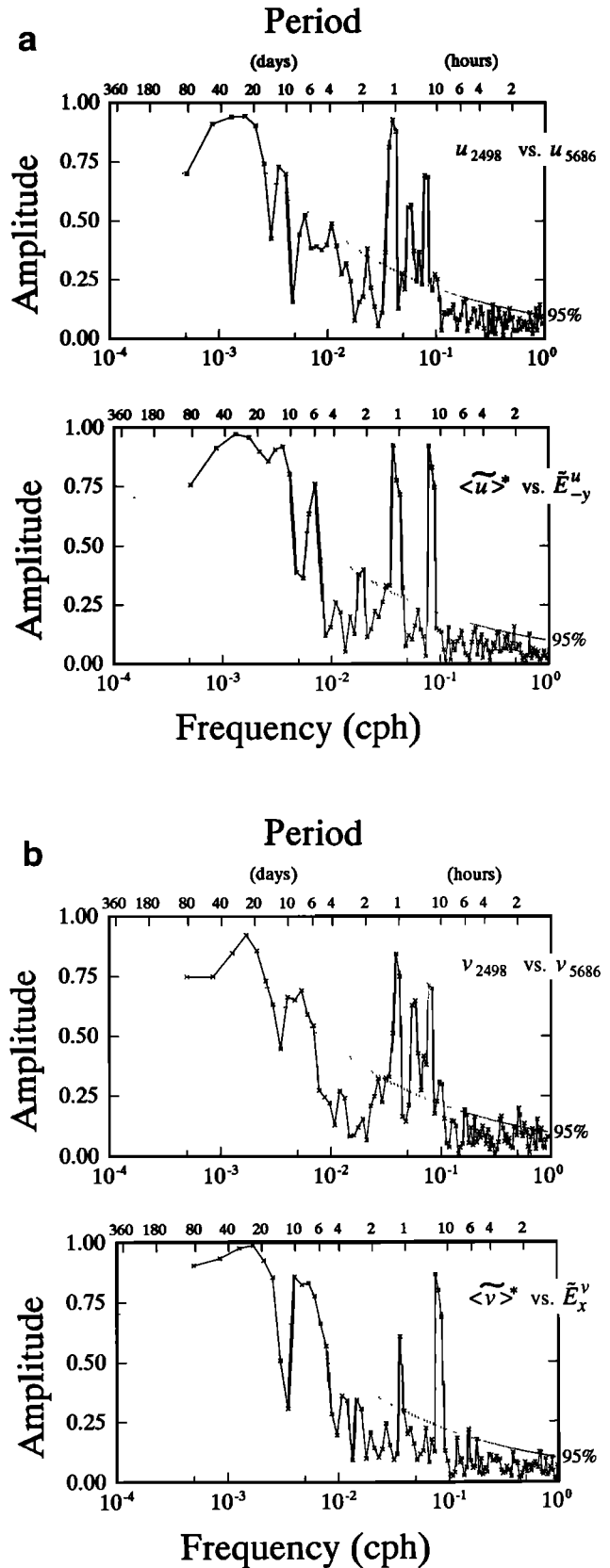

Fig. 11. (a) Coherence amplitude (top) between zonal current measured at 2498 m and the averaged zonal current from the two near-bottom current meters on the BEMPEX mooring, and (bottom) between $\langle\widetilde{u}\rangle^*$ and $\tilde{E}_{-y}^u$ (as in Figue 7a). The plots follow the conventions introduced in Figure 7. Note that the minima in the coherence amplitudes coincide at periods greater than 5 days. (b) As in Figure 11a, but for meridional components.

ling, since there is also weak vertical coherence between the topmost instruments where stalling is minimal (e.g., Figure 10). Rotor stalling certainly adds noise to the deepest instruments while reducing the total variance observed (e.g., Figure 5), but the most important factor is probably a complex vertical structure for the oceanic motion in some frequency bands. For the shorter vertical correlation lengths in these bands, a small number of widely spaced instruments in the vertical is not adequate for sampling the velocity structure and accurately deriving $<\widetilde{v}_h>^*$. This hypothesis leads to important negative conclusions about the ability to accurately observe transport fluctuations or barotropic variability with current meter moorings. However, current meter moorings may not generally be all that bad, since those frequency bands enumerated earlier that had the weakest vertical coherence also corresponded to relative minima in the power spectra of the horizontal currents (e.g., Figure 12). In other words, the mooring does a poor job of determining $<\widetilde{v}_h>^*$ or barotropic currents in BEMPEX primarily where the fluctuations are weakest and presumably least interesting.

A meaningful estimate of C in (1) cannot be produced by comparing $\bar{E}_h$ with $<\widetilde{v}_h>^*$, because of the unknown loss of variance in the latter from current meter rotor stalls. However, transfer functions between $\bar{E}_h$ (multiplied by $-1/F_z$ to get units of velocity) and $<\widetilde{v}_h>^*$ were calculated and averaged across those frequency bands with significant coherence (at the 95% level; see Figure 7) to obtain empirical scale factors to correct for the loss of variance in $<\widetilde{v}_h>^*$, thus facilitating further comparisons with $\bar{E}_h$; this is equivalent to assuming C in (1) is unity and scaling the estimate of (2) to achieve that value. The multiplicative scale factors for $<\widetilde{u}>^*$ and $<\widetilde{v}>^*$ are 1.48 and 1.61, respectively. The large size of these empirical scale factors is not surprising, since the instruments below 1000 m, for which up to 35% of the observations were zero on account of the rotor stalls, provide the velocity estimates for 70% of the depth range in (3). Figures 12 and 13 compare power spectra and low-pass-filtered time series of the scaled version of $<\widetilde{v}_h>^*$ with $\bar{E}_h$ (the latter, in volts per meter, is converted to units of velocity, meters per second, by division by $-F_z=0.000035954$ Tesla). The good spectral agreement in Figure 12 and the high visual correlation in Figure 13 (correlation coefficients are greater than 0.86 for both components) further support the interpretation of the HEF given by (1). However, the present intercomparison cannot be considered definitive due to an inability to estimate a data-based value of C.

While mooring motion can result in underestimates of barotropic current amplitudes [e.g., Howe and Munk, 1988], the BEMPEX mooring experienced very little motion, with the largest displacements being the result of inertial-internal wave currents. For the 3-m maximum subinertial vertical deflection of the top of the mooring (see section 3), the implied maximum horizontal deflection at the mooring apex by subinertial currents is 185 m. If the mooring traced a watch circle with this radius in 4 days, the speed of the mooring apex would be 3.4 mm s^{-1}, which is the amount the observed speed would be reduced relative to the true water speed. For longer periods and at deeper depths, the watch circle speed is proportionately smaller. At the most energetic periods (20–40 days; Figure 12), the speed of the mooring apex would be much less than 1 mm s^{-1}. The small size of these worst-case scenario estimates suggests that mooring motion is unlikely to have contributed significantly to the underestimation of $<\widetilde{v}_h>^*$. Furthermore, the only significant subinertial coherence between $<\widetilde{v}_h>^*$ and the pressure
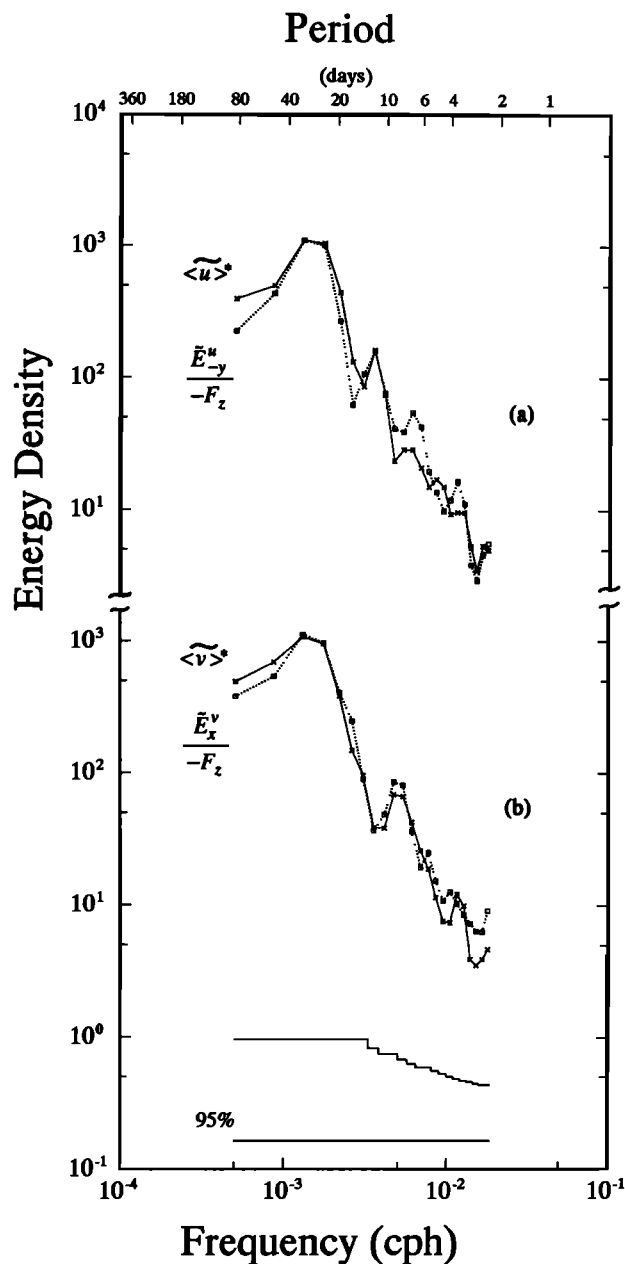
Fig. 12. (a) Power spectra of $<\widetilde{u}>^*$ scaled as described in the text (solid line with crosses), and $\bar{E}^u_{-y}/(-F_z)$ (dotted line with squares), plotted following the conventions introduced in Figure 5. (b) As in Figure 12a, but for $<\widetilde{v}>^*$ and $\bar{E}^v_x/(-F_z)$.

fluctuations recorded at 70 m and 293 m occurred at 20–40 days where the coherence between $<\widetilde{v}_h>^*$ and $\bar{E}_h$ was strongest. Consequently, mooring motion is not a likely source of significant noise in $<\widetilde{v}_h>^*$.

The validity of the scale factors presented above can be checked by comparing barotropic tidal currents estimated from the moored measurements with acoustic estimates of the zonal barotropic tidal currents [Worcester et al. 1990], and with numerical model predictions of tidal currents [e.g., Schwiderski, 1980]. The barotropic currents, v_h^{bt}, were estimated by projecting the moored current meter data onto the gravest vertical structure function appropriate for horizontal currents at low frequencies (with respect to the buoyancy frequency [e.g., LeBlond
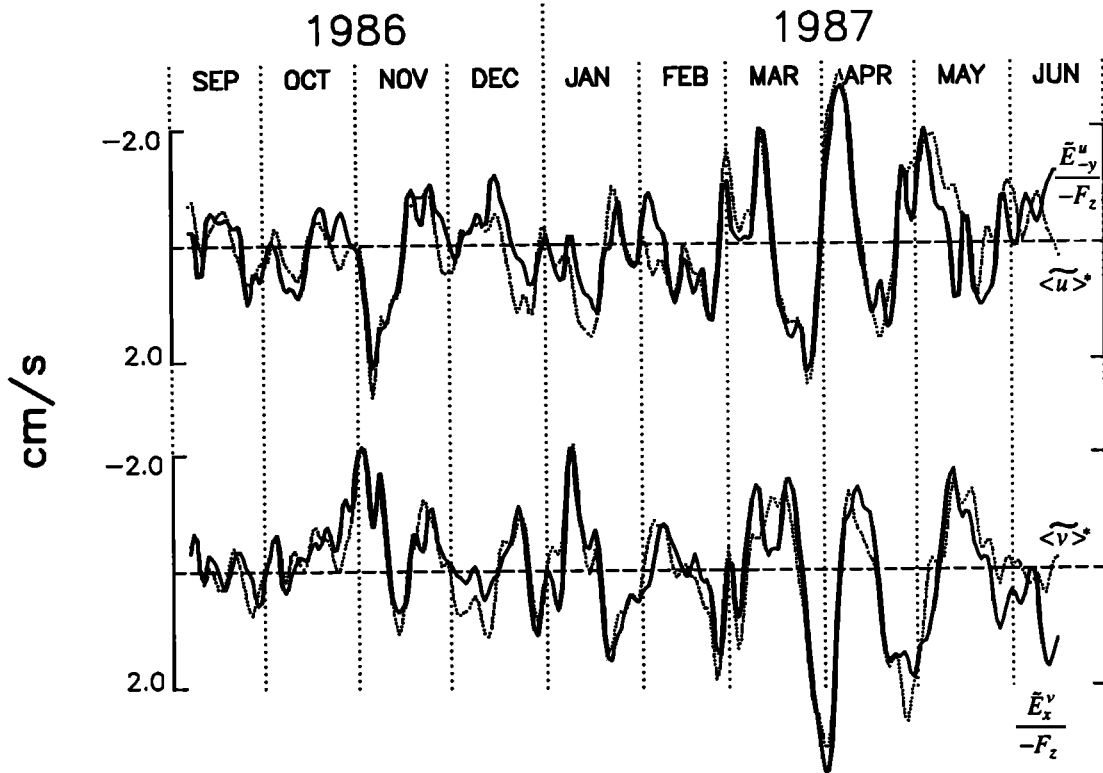
Fig. 13. (Top) Time series of low-pass-filtered (3 dB at 2.7 days, 20 dB at 1.6 days) $<\tilde{u}>^*$ scaled as described in the text (dotted line), and $\tilde{E}^u_{-y}/(-F_z)$ (solid line). The means have been subtracted from the time series before plotting. The root-mean-square (rms) difference between the two traces is 0.48 cm s^{-1}. (Bottom) Time series of low-pass-filtered $<\tilde{v}>^*$ scaled as described in the text (dotted line), and $\tilde{E}^v_x/(-F_z)$ (solid line). The means have been subtracted from the time series before plotting. The rms difference between the two traces is 0.46 cm s^{-1}.

TABLE 3. Comparison of Observed and Numerically Predicted Barotropic Tidal Currents at the BEMPEX Mooring

Constituent Name	Period, hours	Amplitude, cm s^{-1}				Greenwich Phase, G°		
		Mooring*	Corrected*	Acoustic†	Schwiderski‡	Mooring*	Acoustic†	Schwiderski‡
			Zonal Barotropic Component u^{bt}					
O$_1$	25.82	0.31 ± 0.04	0.46 ± 0.05	0.46 ± 0.05	0.33	122 ± 7	101 ± 3	99
K$_1$	23.94	0.50 ± 0.04	0.74 ± 0.06	0.72 ± 0.09	0.45	135 ± 5	128 ± 9	127
N$_2$	12.66	0.10 ± 0.06	0.15 ± 0.09	0.18 ± 0.06	0.16	216 ± 35	194 ± 37	184
M$_2$	12.42	0.89 ± 0.06	1.32 ± 0.09	1.28 ± 0.13	1.29	218 ± 4	221 ± 5	222
S$_2$	12.00	0.36 ± 0.07	0.53 ± 0.10	0.52 ± 0.09	0.66	280 ± 11	268 ± 15	270
			Meridional Barotropic Component v^{bt}					
O$_1$	25.82	0.16 ± 0.02	0.26 ± 0.04	NA	0.34	227 ± 8	NA	218
K$_1$	23.94	0.24 ± 0.02	0.39 ± 0.04	NA	0.59	229 ± 6	NA	228
N$_2$	12.66	0.17 ± 0.06	0.27 ± 0.09	NA	0.18	182 ± 19	NA	171
M$_2$	12.42	0.66 ± 0.06	1.06 ± 0.09	NA	1.16	170 ± 5	NA	180
S$_2$	12.00	0.32 ± 0.05	0.52 ± 0.08	NA	0.61	210 ± 9	NA	197

NA, not available.

*Corrected amplitude is the mooring amplitude multiplied by the scale factors 1.48 and 1.61 for the zonal and meridional currents, respectively. Both amplitudes have been corrected for the amplitude beat due to the 18.6 year period of the regression of the lunar node [Schureman, 1958]; the largest correction is an 18% reduction in O$_1$ amplitude. The 95% confidence intervals for the mooring amplitude, corrected amplitude, and mooring Greenwich phase have been estimated following Munk and Cartwright [1966, Appendix B] with a modification to explicitly account for the uncertainties in the estimated noise variances.

† Taken from Worcester et al. [1990] and corrected for the amplitude beat due to the regression of the lunar node. The confidence intervals are standard deviations of the estimates.

‡Schwiderski (private communication to W. Munk, 1988) numerical model estimates.

and Mysak, 1978, section 15]). Structure functions were computed numerically using an average buoyancy frequency profile derived from the September 2, 1986, and May 16, 1987, CTD data collected near the BEMPEX mooring. Amplitudes for five major tidal constituents were estimated from the barotropic current time series by a straightforward Fourier analysis, with subsequent correction for the amplitude beat caused by the 18.6-year period of the regression of the lunar node [e.g., *Schureman*, 1958]. (Note that just for this estimation of tidal constituents, all 12.5 months of current meter data were employed.) The observed tidal current amplitudes are presented in Table 3, alongside both *Worcester et al.*'s [1990] acoustic estimates of zonal tidal currents averaged over a range of 740 km bracketing the BEMPEX mooring and Schwiderski's (private communication to W. Munk, 1988) numerical predictions for the region corresponding to the acoustic estimates. Of the 10 observed "mooring" amplitudes that can be compared with Schwiderski's predictions, seven are well below Schwiderski's. After application of the multiplicative scale factors presented above, these seven observations are all much closer to, with only one exceeding, Schwiderski's predictions. There are also three observed values that are close to Schwiderski's predictions prior to application of the scale factors, only one of which (zonal current for K_1) is substantially greater than Schwiderski's prediction after multiplication by the scale factor. Acoustic estimates (Table 3) of the zonal barotropic tidal currents are in excellent agreement with the corrected "mooring" amplitudes in Table 3 and confirm the larger amplitude of the mooring estimate of K_1 zonal current, compared with Schwiderski's. In all, the tidal current estimates support the conclusion that the moored current meters in BEMPEX yield substantially underestimated barotropic currents. Note that phases are also presented in Table 3, with rather good agreement between observed and numerically calculated values.

5. MEANS AND ANNUAL CYCLES

The reduced coherence amplitudes (relative to the coherence maxima at 20-30 days) between $<\tilde{v}_h>^*$ and $\tilde{E}_h$ at the longest periods in Figure 7, which mirror the reduced vertical coherences between current meters in Figure 11, suggest the need for a closer examination of the lowest frequency components of the data. A straightforward multiple linear regression was employed to estimate means and annual cycle variability from the components of $\tilde{E}_h/(-F_z)$ and $<\tilde{v}_h>^*$ (after correction with the multiplicative scale factors introduced in section 4). The results are shown in Table 4, along with standard error estimates that

TABLE 4. Multiple Linear Regression Estimates of Means and Annual Cycles of $\tilde{E}_h$ and $<\tilde{v}_h>^*$, With Standard Errors

	Annual Cycle		Mean, cm s^{-1}
	Amplitude, cm s^{-1}	Phase, deg	
$\tilde{E}_{-y}^u/-F_z$ [a]	0.24 ± 0.08	-190 ± 36	-0.47 ± 0.10
$<\tilde{u}>^*$	0.46 ± 0.14	-196 ± 22	0.67 ± 0.13 (0.45 ± 0.09) [b]
$\tilde{E}_x^y/-F_z$ [a]	0.37 ± 0.11	-51 ± 15	0.11 ± 0.09
$<\tilde{v}>^*$	0.28 ± 0.21	-87 ± 12	0.42 ± 0.13 (0.26 ± 0.08) [b]

[a] $-F_z$ = 35,954 nT.

[b] Not corrected for reduction of variance due to rotor stalls.

take into account the reduction in the degrees of freedom of the data due to their non-zero integral time scales. The latter ranged from 2.5 to 6 days.

The amplitudes and phases of the east and north components of the annual cycle in Table 4 are in fairly good agreement, given the sizes of the standard errors. The means, however, exhibit greater disparity, especially the zonal means. Since it can be argued that the empirical scale factors (that were successfully employed to correct the fluctuations in $<\tilde{v}_h>^*$ for the reduction in variance due to rotor stalling) are not appropriate for adjusting the means for bias due to the rotor stalling, the unscaled means are also shown in Table 4. The unscaled mean meridional velocity estimate from the current meter mooring is now within one standard error of the mean meridional velocity estimated from the electric field. The zonal mean velocity estimates, however, still differ by approximately 1 cm s^{-1}, significant at 5 standard errors, and are in opposite directions. While a definitive explanation for this discrepancy has not been found, the plausibility of several explanations can be evaluated.

Some idea of the possible bias from rotor stalling that may have occurred in the deeper current meter data sets is obtained from the zonal mean currents at 5650 m and 5722 m that are in opposite directions and differ by 0.25 cm s^{-1}, although this difference is significant at only 1.5 standard errors. However, to account for the observed discrepancy of 1 cm s^{-1} in mean depth-averaged zonal currents (Table 4), the deepest three instruments (which had significant rotor stalling) would each have to have had an eastward bias of over 1 cm s^{-1}, which is doubtful considering that the rms variability at each of these instruments was only around 3 cm s^{-1} (after application of the empirical scale factors). If any of the instruments had a smaller bias, a proportionately larger bias would have to be conjectured for the other instruments. Such large biases are unlikely.

Certainly, the discrete approximations in equation (3) to the vertical integrals in (2) will produce biased estimates of the conductivity-weighted, vertically averaged mean currents. The large instrument separations on the current meter mooring have already been shown to be the most likely cause of the discrepancies between $<\tilde{v}_h>^*$ and $\tilde{E}_h$ in several narrow period bands between 2 days and 90 days. If the trapezoidal rule is applied to the 173-m and 943-m currents without the modification introduced in section 4, the discrepancies in the mean current estimates in Table 4 grow by 0.3 and 0.2 cm s^{-1} for the zonal and meridional components, respectively. It is not at all unreasonable to suppose that a deep westward maximum in current was missed by the discrete vertical sampling, given the vertical structures of mean zonal currents revealed by other moored current measurements in the central-eastern Pacific [e.g., *Earle*, 1975; *Hu and Niiler*, 1987; *Niiler and Hall*, 1988]. But to account for the 1 cm s^{-1} discrepancy in depth-averaged zonal current estimates, westward currents of over 2 cm s^{-1} would have to be sandwiched between the 943-m and 2498-m depths or between the 2498-m and 5650-m depths. There is no evidence that such large mean currents in such vertically restricted depth ranges exist. Note that the observed mean zonal currents, i.e., 0.74 ± 0.22, -0.05 ± 0.12, -0.08 ± 0.08 and 0.18 ± 0.10 cm s^{-1} for 943 m, 2498 m, 5650 m, and 5722 m, respectively, do not suggest the existence of such relatively strong currents.

Since the mean barotropic currents can be expected to follow planetary vorticity (f/H) contours, more or less faithfully depending on the strength of direct atmospheric forcing, it is not unreasonable to suppose that the mean barotropic currents are quite spatially variable in the BEMPEX region that consists of

low abyssal hills with 100-m depth changes over 5-km distances. Under such a supposition, it does not seem so odd that a point estimate of depth-averaged water velocity from a current meter mooring should differ from a horizontal average (over at most a 12- to 18-km-wide region) of the same quantity centered 6 km to the south. But, is a difference of 1 cm s^{-1} reasonable? There are no data to explicitly answer this question. However, moored current measurements made by *Taft et al.* [1981] in a region of the North Pacific (approximately 30°N, 158°W) with similar topographic variability provide some information on the spatial variability of deep ocean currents in the North Pacific, and, by inference, on the spatial variability of the barotropic flow. Nine-month means of currents measured 100 m off the bottom, and separated by 29 km, differed in direction and with 1 cm s^{-1} magnitude for both horizontal components. The instruments that provided these means (VACMs M12 and M14 of *Taft et al.* [1981]) had relatively low numbers of rotor stalls (21% and 36% zero speeds) compared with other instruments in the experiment. A Geodyne 850 current meter (M16, with only 22% zero speeds) 95 km to the southeast of M14 had means differing from M14 by approximately 3 cm s^{-1} in each component. To go from these examples of 1 cm s^{-1} variation over 30 km to a variation of 1 cm s^{-1} over 5–10 km, which is needed to justify the zonal mean current discrepancy in Table 4, is still a large extrapolation, but not an implausibly large one given the small spatial scale over which the topography varies in BEMPEX (Figure 2).

Finally, the electric field sensor EB, from which the mean current estimates in Table 4 were derived, was calibrated before and after recovery and displayed no flaws. On the seafloor, EB was oriented 128° relative to geographic north, so that the signals from both salt bridges contributed similar proportions to both east-west and north-south electric field observations. Therefore the small discrepancy between the mean meridional current estimates in Table 4 precludes the electrometer from being the source of the much larger discrepancy between the mean zonal current estimates.

6. VERTICAL MODE CONTRIBUTIONS TO E_h

The conductivity and horizontal water velocity in (2) can be expanded in terms of any convenient, orthogonal set of vertical basis functions. For a simple demonstration of the minor role that depth-dependent (baroclinic and nongeostrophic) fluctuations play in $<\widetilde{v_h}>^*$ (and hence $\bar{E}_h$) at the BEMPEX site, the currents and conductivity will be assumed to consist of a depth-independent component plus a depth-dependent residual. Equation (2) then reduces to the sum of a depth-independent water velocity, $<v_h>$, plus a conductivity-weighted vertical average of the residual currents. The velocity $<v_h>$ is estimated with the discrete approximation in (3) by setting the conductivity equal to 1. The estimate is called $<\widetilde{v_h}>$. The estimated contribution to (2) from baroclinic and other depth-dependent variability, called $<\widetilde{v_h^{bc}}>^*$, is then simply the difference between $<\widetilde{v_h}>^*$ and $<\widetilde{v_h}>$.

Figure 14 shows power spectra of the components of $<\widetilde{v_h}>$ and $<\widetilde{v_h^{bc}}>^*$ after multiplication by the empirical scale factors discussed at the end of section 4. The spectra of $<\widetilde{v_h}>$ are indistinguishable from the spectra of $<\widetilde{v_h}>^*$ (Figure 12), because $<\widetilde{v_h^{bc}}>^*$ is so weak. Even using an extreme time-mean profile of conductivity taken from *Levitus* [1982], which is appropriate for one corner of the BEMPEX array and has greater conductivity

variability with depth than at the BEMPEX mooring, increases the power in $<\widetilde{v_h^{bc}}>^*$ only by a factor of 3 (Figure 14). This is still insignificant compared with $<\widetilde{v_h}>$.

A more formal decomposition of the time-dependent moored current meter data and time-independent CTD conductivity data was accomplished by projecting them onto the dynamical vertical structure functions appropriate for horizontal currents at low frequencies (see section 4). Estimation of $<v_h>^*$ in (2) can then be accomplished by a straightforward combination of the modal amplitude coefficients. The root-mean-square (rms) values of the low-pass-filtered (3-dB point at 2.7 days, 20-dB point at 1.6 days) amplitude coefficient time series for currents are shown in Table 5, alongside the amplitude coefficients for the conductivity. A straightforward combination of the amplitude coefficients in Table 5 suggests a baroclinic contribution to $<\widetilde{v_h}>^*$ of about 5% in rms amplitude for both horizontal components, which translates into much less than a 1% contribution to the energy in $<\widetilde{v_h}>^*$ (assuming the individual modes are uncorrelated), in agreement with the power spectra of $<\widetilde{v_h^{bc}}>^*$ presented in Figure 14. The estimated barotropic contribution to $<\widetilde{v_h}>^*$, called $\widetilde{v_h^{bt}}$, is nearly indistinguishable from $<\widetilde{v_h}>$ (i.e., component mean square differences less than 2% of component variances) but is slightly (1–2%) less coherent with $<\widetilde{v_h}>^*$ than is $<\widetilde{v_h}>$.

The correlation coefficients between the low-pass-filtered estimates of conductivity-weighted, vertically averaged water velocity ($<\widetilde{v_h}>^*$), vertically averaged water velocity ($<\widetilde{v_h}>$), and barotropic water velocity ($\widetilde{v_h^{bt}}$) are given in Table 6. Also shown in Table 6 are the correlation coefficients between these estimates of water velocity and $\bar{E}_h$. The small variation of conductivity with depth in the BEMPEX area, ranging from 4.0 S m^{-1} near the surface to 3.2 S m^{-1} at the bottom, combined with the relatively strong barotropic currents (as shown by Table 5), results in such small baroclinic contributions to $<\widetilde{v_h}>^*$ that $<\widetilde{v_h}>^*$ is nearly indistinguishable from $<\widetilde{v_h}>$ and is not obviously better related to $\bar{E}_h$ than is $<\widetilde{v_h}>$, according to Table 6. Furthermore, there is only a small difference between vertically averaged water velocity $<\widetilde{v_h}>$ and the barotropic water velocity $\widetilde{v_h^{bt}}$ according to Table 6, so that the barotropic water velocity is almost as strongly correlated with $\bar{E}_h$ as are $<\widetilde{v_h}>^*$ and $<\widetilde{v_h}>$. Consequently, the horizontal electric field is an accurate barotropic current sensor in the BEMPEX area at periods greater than a few days.

7. SUMMARY

High coherence between estimates of E_h and $<v_h>^*$ at periods greater than 5 days (Figure 7) has been interpreted as strong support for the validity of equations (1) and (2), where N≈0. However, since the estimates $<\widetilde{v_h}>^*$ and $<\widetilde{v_h}>$ are indistinguishable (Table 6), the dependence of E_h on conductivity weighting (required by Maxwell's equations) in the vertical integral of velocity has not been demonstrated.

The lack of perfect coherence between the estimates $\bar{E}_h$ and $<\widetilde{v_h}>^*$ has been shown to be principally the result of inaccuracies resulting from estimating $<v_h>^*$ with a small number of widely separated measurements. Specifically, the lack of vertical coherence between current meters (Figures 10 and 11) hinders the accurate estimation of $<v_h>^*$. This incoherence is probably the result of a fairly complex vertical structure of the motion in some period bands but is also due in some part to bearing friction that produces at least the numerous rotor stalls for the instruments below 1000 m. Externally generated electric fields
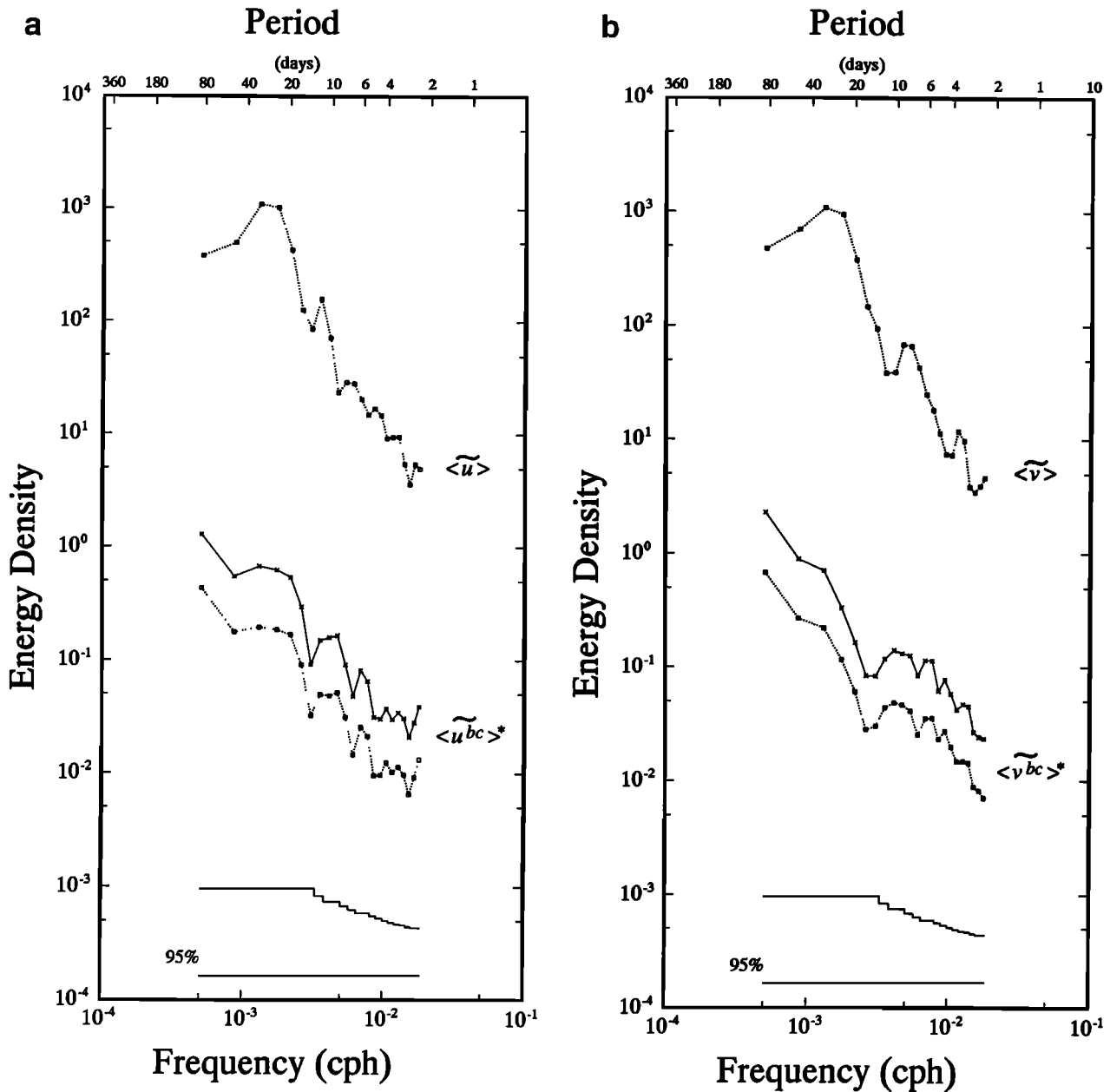
Figure 14. (*a*) Power spectra of $\widetilde{u}$ (upper dotted line with squares) and $\langle\widetilde{u^{bc}}\rangle^*$. The latter is calculated assuming a seawater conductivity profile representative of the neighborhood of the BEMPEX mooring during the experiment (lower dotted line with squares) and alternately assuming an extreme conductivity profile calculated with climatological temperatures and salinities [*Levitus*, 1982] appropriate for one corner of the BEMPEX array (solid line with crosses). All three time series were multiplied by the empirical scale factor (see section 4 of the text) prior to estimation of the power spectra. The spectra are plotted following the conventions introduced in Figure 5. (*b*) As in Figure 14*a*, but for $\langle\widetilde{v}\rangle$ and $\langle\widetilde{v^{bc}}\rangle^*$.

are not an important noise at periods greater than 2 days, since they are generally small (Figure 9) and can be removed from the data using frequency domain correlation or time domain adaptive cancellation techniques, where the magnetic field (which contains no detectable motional component at periods greater than 2 days; e.g., Figure 8*b*) provides a measure of this noise.

The lack of agreement between the amplitudes of $\bar{E}_h/(-F_z)$ and $\langle\widetilde{v_h}\rangle^*$ appears to have been the result of rotor stalling below 1000 m (with perhaps some small contribution to the disagreement from mooring motion). Independently corroborated scale factors were employed to increase the component

amplitudes of $\langle\widetilde{v_h}\rangle^*$ by approximately 50%, in order to achieve the component amplitudes of $\bar{E}_h/(-F_z)$. Consequently, the data can not be used to estimate the constant of proportionality, C in (1), and it has been assumed to be equal to 1.

Some of the disagreements noted above are possibly due to the fact that $\mathbf{E}_h$ is an average of $\langle v_h\rangle^*$ over a horizontal distance of no more than 2 to 3 times the water depth (approximately 12 to 18 km in BEMPEX). In particular, the lack of agreement between the zonal means, discussed in section 5, is suggested to be the result of $\bar{E}_h$ being a horizontal average, centered 6 km south of the BEMPEX mooring, of spatially variable barotropic currents.

TABLE 5. Vertical Mode Amplitude Coefficients for Conductivity* and Moored Horizontal Currents

	Root-Mean-Square Amplitude, cm s^{-1}		Conductivity, S m^{-1}
Mode	Zonal Current	Meridional Current	
1	0.840	0.660	3.206
2	1.287	0.937	−0.100
3	0.619	0.412	−0.078
4	0.300	0.364	−0.017

* Averaged from two CTD profiles near the mooring.

8. FINAL REMARKS

The minimal contribution of baroclinic currents to the HEF, which also resulted in the equivalence of $<\tilde{v_h}>^*$, $<\tilde{v_h}>$, and $\tilde{v_h^{bt}}$, is not unique to the BEMPEX area. Table 1 and *Chave and Luther* [1990] show that the probable impact of baroclinic currents on the HEF is quite small for a number of representative oceanic locations, so that the HEF serves as an efficient barotropic current meter. However, it should not be assumed that HEF data are useless in the uncommon locations (e.g., the major axis of the Gulf Stream north of Cape Hatteras) where baroclinicity is strong enough to produce important effects in the HEF. As long as the conductivity structure is known, the HEF constitutes a direct integral measurement of the horizontal water velocity with known modal weighting which gives it a distinct advantage over point measurements in a number of applications. For instance, such integral measures may be more useful for validating numerical model simulations than are point measurements.

Horizontal electrometers do not suffer from either rotor stall problems in weak mean flows or mooring motion contamination

TABLE 6. Summary of Correlation Coefficients Among the Low-Pass-Filtered Water Velocity Estimates and Between These Estimates and $\tilde{E}_h$

	Horizontal Components			
	$\tilde{E}^u_{-y}$	$<\tilde{u}>^*$	$<\tilde{u}>$	$\tilde{u}^{bt}$
$\tilde{E}^u_{-y}$	1.0	0.865	0.867	0.842
$<\tilde{u}>^*$	0.865	1.0	0.9998	0.995
$<\tilde{u}>$	0.867	0.9998	1.0	0.993
$\tilde{u}^{bt}$	0.842	0.995	0.993	1.0

	Meridional Components			
	$\tilde{E}^v_x$	$<\tilde{v}>^*$	$<\tilde{v}>$	$\tilde{v}^{bt}$
$\tilde{E}^v_x$	1.0	0.884	0.882	0.879
$<\tilde{v}>^*$	0.884	1.0	0.9997	0.993
$<\tilde{v}>$	0.882	0.9997	1.0	0.991
$\tilde{v}^{bt}$	0.879	0.993	0.991	1.0

$\tilde{E}^u_{-y}$ and $\tilde{E}^v_x$ are estimates of the horizontal electric field components, $<\tilde{u}>^*$ and $<\tilde{v}>^*$ are estimates of the conductivity-weighted, vertically averaged horizontal water velocity components, $<\tilde{u}>$ and $<\tilde{v}>$ are estimates of the vertically averaged horizontal water velocity components, and $\tilde{u}^{bt}$ and $\tilde{v}^{bt}$ are estimates of the barotropic water velocity components.

in the presence of strong currents. In addition, horizontal electrometers are inexpensive to construct and deploy compared to current meter moorings. This makes them especially attractive for exploring the barotropic structure of the ocean, for monitoring the transport of key ocean currents, and where spatial (wavenumber) information from dense clusters of sensors is desired. The large number of moorings required to study such problems is often prohibitively expensive, and can lead to the temptation to underinstrument individual moorings, yielding potential vertical resolution problems and misleading results. The low power requirements, low cost, and ease of deployment of electrometers also makes them viable candidate instruments for long-term monitoring applications. Consequently, it is not an exaggeration to state that electrometers are valuable oceanographic tools that are underutilized at present.

APPENDIX: MAGNETOTELLURIC TRANSFER FUNCTIONS

The magnetotelluric (MT) transfer functions are obtained [e.g., *Vozoff*, 1972] by employing Maxwell's equations to calculate the ratios of externally produced electric and magnetic fields at the seafloor, given a model of the conductivity of the Earth and assuming electric displacement currents are small in the Earth. The horizontally homogeneous conductivity model used to calculate the MT transfer functions, which led to the estimates of the externally-generated electric fields at the seafloor shown in Figure 9, is given in Table A1. The top three layers, which have almost no effect on the electromagnetic fields at periods greater than 1 hour, are justified by *Chave et al.* [1990a] on the basis of controlled source EM, laboratory and MT data. The fourth layer is based on an average of oceanic MT data discussed by *Oldenburg et al.* [1984]. The fifth layer is difficult to constrain with oceanic data because of the increasing oceanic signals in the electric field at periods greater than 2 days, so an inversion of data from the Hawaiian Islands given by *Parker and Whaler* [1981] was used. The half-space conductivity at the bottom was estimated from global magnetic sounding data [*Parker*, 1970].

TABLE A1. Layered Conductivity Model of the Earth

Conductivity, S m^{-1}	Thickness, km
0.005	6.5
0.00001	30
0.003	40
0.1	220
0.6	200
1.0	half-space

The layers are ordered from shallowest to deepest.

The predicted electric field spectra in Figure 9 are not strongly dependent on the model conductivity profile. At periods greater than 2 days, the spectra are dependent only on the conductivity below 200 km. While the latter is not known to better than a factor of 2–5, such variations only cause factor of 2 changes in the calculated low-frequency electric field spectra. Many global sounding studies suggest higher conductivities below 600 km depth than given in Table A1. Certainly, the core is at least 1000 times more conductive. Increasing the model's deep conductivities decreases the calculated electric field at long periods at the seafloor. The shallower the change, the shorter the period affected.

REFERENCES

Armi, L., and E. D'Asaro, Flow structures of the benthic ocean, *J. Geophys. Res.*, *85*, 469–484, 1980.

Chave, A. D., and D. S. Luther, Low-frequency, motionally induced electromagnetic fields in the ocean, 1, Theory, *J. Geophys. Res.*, *95*, 7185–7200, 1990.

Chave, A. D., J. H. Filloux, D. S. Luther, L. K. Law, and A. White, Observations of motional electromagnetic fields during EMSLAB, *J. Geophys. Res.*, *94*, 14,153–14,166, 1989.

Chave, A. D., A. Flosadóttir, and C. S. Cox, Some comments on seabed propagation of ULF/ELF electromagnetic fields, *Radio Sci.*, *25*, 825–836, 1990a.

Chave, A. D., D. S. Luther, and J. H. Filloux, Spatially-averaged velocity from the seafloor horizontal electric field, *Proc. IEEE Working Conf. Current Meas.*, *4th*, 46–53, 1990b.

Cox, C. S., J. H. Filloux, P. I. Gough, J. C. Larsen, K. A. Poehls, R. P. von Herzen, and R. Winter, Atlantic lithosphere sounding, *J. Geomagn. Geoelectr.*, *32*, Suppl., SI13–SI32, 1980.

Earle, M. D., Current measurements in the eastern central North Pacific Ocean, *Deep Sea Res.*, *22*, 875–881, 1975.

Filloux, J. H., Instrumentation and experimental methods for oceanic studies, *Geomagnetism*, vol. 1, edited by J. A. Jacobs, pp. 143–248, Academic, San Diego, Calif., 1987.

Fofonoff, N. P., Dynamics of ocean currents, in *The Sea*, vol. 1, edited by M. N. Hill, pp. 323–395, John Wiley, New York, 1962.

Fofonoff, N. P., and R. C. Millard, Algorithms for computation of fundamental properties of sea water, *UNESCO Tech. Pap. Mar. Sci.*, *44*, 53 pp., 1983.

Hogg, H. G., Evidence for baroclinic instability in the Gulf Stream recirculation, *Prog. Oceanogr.*, *14*, 209–229, 1985.

Horne, R. A., *Marine Chemistry*, 568 pp., Wiley-Interscience, New York, 1969.

Howe, B. M., and W. H. Munk, Deep sea moorings in a tidal current, *Deep Sea Res.*, *35*, 111–119, 1988.

Hu, J.-H., and P. P. Niiler, NEPAC current meter and XBT data, technical report, *SIO Ref. 87-4*, 187 pp., Scripps Inst. of Oceanogr., La Jolla, Calif., 1987.

Larsen, J. C., Electric and magnetic fields induced by deep sea tides, *Geophys. J. R. Astron. Soc.*, *16*, 47–70, 1968.

Larsen, J. C., and T. B. Sanford, Florida Current volume transports from voltage measurements, *Science*, *227*, 302–304, 1985.

LeBlond, P. H., and L. A. Mysak, *Waves in the Ocean*, 602 pp., Elsevier, New York, 1978.

Levitus, S., Climatological atlas of the world ocean, *NOAA Prof. Pap 13*, 173 pp., U.S. Govt. Print. Off., Washington, D. C., 1982.

Luther, D. S., A. D. Chave, and J. H. Filloux, BEMPEX: A study of barotropic ocean currents and lithospheric electrical conductivity, *EOS Trans. AGU*, *68*, 618–619, 628–629, 1987.

Luther, D. S., A. D. Chave, J. H. Filloux, and P. F. Spain, Evidence for local and nonlocal barotropic responses to atmospheric forcing during BEMPEX, *Geophys. Res Lett.*, *17*, 949–952, 1990.

Müller, P., and C. Frankignoul, Direct atmospheric forcing of geostrophic eddies, *J. Phys. Oceanogr.*, *11*, 287–308, 1981.

Munk, W. H., and D. E. Cartwright, Tidal spectroscopy and prediction, *Philos. Trans. R Soc. London, Ser. A*, *259*, 533–581, 1966.

Niiler, P. P., and M. M. Hall, Low-frequency eddy variability at 28°N, 152°W in the eastern North Pacific subtropical gyre, *J. Phys. Oceanogr.*, *18*, 1670–1685, 1988.

Niiler, P. P., and C. J. Koblinsky, A local time-dependent Sverdrup balance in the eastern North Pacific Ocean, *Science*, *229*, 754–756, 1985.

Oldenburg, D. W., K. P. Whittall, and R. L. Parker, Inversion of ocean bottom magnetotelluric data revisited, *J. Geophys. Res.*, *89*, 1829–1833, 1984.

Parker, R. L., The inverse problem of electrical conductivity in the mantle, *Geophys. J. R. Astron. Soc.*, *22*, 121–138, 1970.

Parker, R. L., and K. A. Whaler, Numerical methods for establishing solutions to the inverse problem of electromagnetic induction, *J. Geophys. Res.*, *86*, 9574–9584, 1981.

Sanford, T. B., Motionally-induced electric and magnetic fields in the sea, *J. Geophys. Res.*, *76*, 3476–3492, 1971.

Sanford, T. B., Recent improvements in ocean current measurement from motional electric fields and currents, *Proc. IEEE Working Conf. Current Meas*, *3rd*, 65–76, 1986.

Sanford, T. B., R. G. Drever, and J. H. Dunlap, An acoustic Doppler and electromagnetic velocity profiler, *J Atmos. Ocean. Technol.*, *2*, 110–124, 1985.

Schmitz, W. J., Jr., Observations of the vertical distribution of low frequency kinetic energy in the western North Atlantic, *J. Mar. Res.*, *36*, 295–310,1978.

Schmitz, W. J., Jr., Weakly depth-dependent segments of the North Atlantic circulation, *J. Mar. Res.*, *38*, 111–133, 1980.

Schureman, P., Manual of Harmonic Analysis and Prediction of Tides, *Spec. Publ. 98*, 317 pp., U.S. Coast and Geod. Surv., U.S. Govt. Print. Off., Washington, D. C., 1958.

Schwiderski, E. W., On charting global ocean tides, *Rev. Geophys.*, *18*, 243–268, 1980.

Spain, P., and T. B. Sanford, Accurately monitoring the Florida Current with motionally-induced voltages, *J. Mar. Res.*, *45*, 843–870, 1987.

Taft, B. A., S. R. Ramp, J. G. Dworski, and G. Holloway, Measurements of deep currents in the central North Pacific, *J. Geophys. Res.*, *86*, 1955–1968, 1981.

Vozoff, K., The magnetotelluric method in the exploration of sedimentary basins, *Geophysics*, *37*, 98–141, 1972.

Weller, R., and R. Davis, A vector-measuring current meter, *Deep Sea Res.*, *27*, 565–582, 1980.

Widrow, B., J. R. Glover, Jr., J. M. McCool, J. Kaunitz, C. S. Williams, R. H. Hearn, J. R. Zeidler, E. Dong, Jr., and R. C. Goodlin, Adaptive noise canceling: Principles and applications, *Proc. IEEE*, *63*, 1692–1716, 1975.

Worcester, P. F., B. D. Dushaw, and B. M. Howe, Gyre-scale current measurements using reciprocal acoustic transmissions, *Proc. IEEE Working Conf. Current Meas.*, *4th*, 65–70, 1990.

Wunsch, C., and J. Dahlen, A moored temperature and pressure recorder, *Deep Sea Res.*, *21*, 145–154, 1974.

A. D. Chave, AT&T Bell Laboratories, Murray Hill, NJ 07974.

J. H. Filloux and D. S. Luther, Scripps Institution of Oceanography, Physical Oceanography Research Division, Code 0230, University of California, San Diego, La Jolla, CA 92093.